













TECH BRIEFS

NATIONAL AERONAUTICS AND SPACE ADMINISTRATION

-  **Technology Focus**
-  **Electronics/Computers**
-  **Software**
-  **Materials**
-  **Mechanics/Machinery**
-  **Manufacturing**
-  **Bio-Medical**
-  **Physical Sciences**
-  **Information Sciences**
-  **Books and Reports**

INTRODUCTION

Tech Briefs are short announcements of innovations originating from research and development activities of the National Aeronautics and Space Administration. They emphasize information considered likely to be transferable across industrial, regional, or disciplinary lines and are issued to encourage commercial application.

Availability of NASA Tech Briefs and TSPs

Requests for individual Tech Briefs or for Technical Support Packages (TSPs) announced herein should be addressed to

National Technology Transfer Center

Telephone No. (800) 678-6882 or via World Wide Web at www.nttc.edu

Please reference the control numbers appearing at the end of each Tech Brief. Information on NASA's Innovative Partnerships Program (IPP), its documents, and services is also available at the same facility or on the World Wide Web at <http://ipp.nasa.gov>.

Innovative Partnerships Offices are located at NASA field centers to provide technology-transfer access to industrial users. Inquiries can be made by contacting NASA field centers listed below.

NASA Field Centers and Program Offices

Ames Research Center

Lisa L. Lockyer
(650) 604-1754
lisa.l.lockyer@nasa.gov

Dryden Flight Research Center

Gregory Poteat
(661) 276-3872
greg.poteat@dfrc.nasa.gov

Glenn Research Center

Kathy Needham
(216) 433-2802
kathleen.k.needham@nasa.gov

Goddard Space Flight Center

Nona Cheeks
(301) 286-5810
nona.k.cheeks@nasa.gov

Jet Propulsion Laboratory

Ken Wolfenbarger
(818) 354-3821
james.k.wolfenbarger@jpl.nasa.gov

Johnson Space Center

Michele Brekke
(281) 483-4614
michele.a.brekke@nasa.gov

Kennedy Space Center

David R. Makufka
(321) 867-6227
david.r.makufka@nasa.gov

Langley Research Center

Martin Waszak
(757) 864-4015
martin.r.waszak@nasa.gov

Marshall Space Flight Center

Jim Dowdy
(256) 544-7604
jim.dowdy@msfc.nasa.gov

Stennis Space Center

John Bailey
(228) 688-1660
john.w.bailey@nasa.gov

Carl Ray, Program Executive

Small Business Innovation
Research (SBIR) & Small
Business Technology
Transfer (STTR) Programs
(202) 358-4652
carl.g.ray@nasa.gov

Doug Comstock, Director

Innovative Partnerships
Program Office
(202) 358-2560
doug.comstock@nasa.gov



TECH BRIEFS

NATIONAL AERONAUTICS AND SPACE ADMINISTRATION



5 Technology Focus: Sensors

- 5 Noise-Canceling Helmet Audio System
- 6 Program Analyzes Spacecraft/Ground Radio Links
- 6 Two-Way Communication Using RFID Equipment and Techniques
- 7 Six-Message Electromechanical Display System



9 Electronics/Computers

- 9 Scanning Terahertz Heterodyne Imaging Systems
- 10 Master Clock and Time-Signal-Distribution System
- 11 Synchronous Phase-Resolving Flash Range Imaging
- 12 Integrated Radial Probe Transition From MMIC to Waveguide
- 13 Bar-Code System for a Microbiological Laboratory
- 14 MMIC Amplifier Produces Gain of 10 dB at 235 GHz
- 15 Mapping Nearby Terrain in 3D by Use of a Grid of Laser Spots
- 15 Digital Beam Deflectors Based Partly on Liquid Crystals
- 16 Narrow-Band WGM Optical Filters With Tunable FSRs



19 Software

- 19 Better Finite-Element Analysis of Composite Shell Structures
- 19 Computing Spacecraft-Pointing Vectors for Limb Tracking
- 19 Enhanced Master Controller Unit Tester
- 19 Rover Graphical Simulator



21 Materials

- 21 Increasing Durability of Flame-Sprayed Strain Gauges
- 22 Multifunctional, High-Temperature Nanocomposites
- 23 Multilayer Impregnated Fibrous Thermal Insulation Tiles



25 Manufacturing & Prototyping

- 25 Radiation-Shielding Polymer/Soil Composites
- 25 Film/Adhesive Processing Module for Fiber-Placement Processing of Composites
- 26 Fabrication of Submillimeter Axisymmetric Optical Components



27 Physical Sciences

- 27 Electrochemical Disposal of Hydrazines in Water
- 28 Statistical Model of Evaporating Multicomponent Fuel Drops
- 29 Resistively Heated SiC Nozzle for Generating Molecular Beams
- 29 Compact Packaging of Photonic Millimeter-Wave Receiver
- 30 Diffractive Combiner of Single-Mode Pump Laser-Diode Beams
- 31 Wide-Band, High-Quantum-Efficiency Photodetector



33 Information Sciences

- 33 A Robustly Stabilizing Model Predictive Control Algorithm
- 33 Modeling Evaporation of Drops of Different Kerosenes



35 Books & Reports

- 35 Development of Vapor-Phase Catalytic Ammonia Removal System
- 35 Several Developments in Space Tethers
- 35 Design Concept for a Nuclear Reactor-Powered Mars Rover
- 35 Formation-Initialization Algorithm for *N* Spacecraft
- 36 DNSs of Multicomponent Gaseous and Drop-Laden Mixing Layers Achieving Transition to Turbulence

This document was prepared under the sponsorship of the National Aeronautics and Space Administration. Neither the United States Government nor any person acting on behalf of the United States Government assumes any liability resulting from the use of the information contained in this document, or warrants that such use will be free from privately owned rights.



Noise-Canceling Helmet Audio System

Voice communication is enhanced by digital processing to suppress noise.

John H. Glenn Research Center, Cleveland, Ohio

A prototype helmet audio system has been developed to improve voice communication for the wearer in a noisy environment. The system was originally intended to be used in a space suit, wherein noise generated by airflow of the space-suit life-support system can make it difficult for remote listeners to understand the astronaut's speech and can interfere with the astronaut's attempt to issue vocal commands to a voice-controlled robot. The system could be adapted to terrestrial use in helmets of protective suits that are typically worn in noisy settings: examples include biohazard, fire, rescue, and diving suits.

The system (see figure) includes an array of microphones and small loudspeakers mounted at fixed positions in

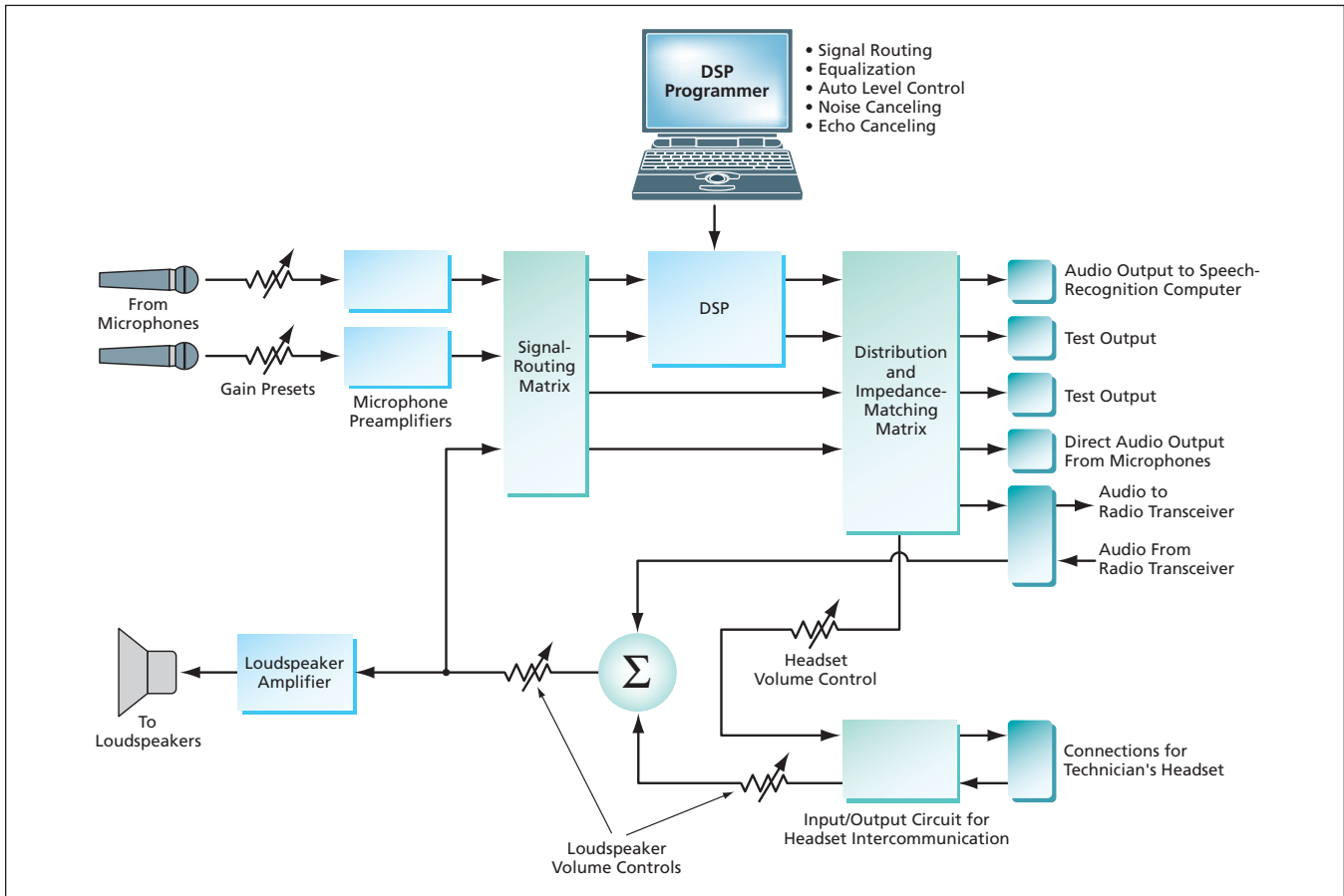
a helmet, amplifiers and signal-routing circuitry, and a commercial digital signal processor (DSP). Notwithstanding the fixed positions of the microphones and loudspeakers, the system can accommodate itself to any normal motion of the wearer's head within the helmet.

The system operates in conjunction with a radio transceiver. An audio signal arriving via the transceiver intended to be heard by the wearer is adjusted in volume and otherwise conditioned and sent to the loudspeakers. The wearer's speech is collected by the microphones, the outputs of which are logically combined (phased) so as to form a microphone-array directional sensitivity pattern that discriminates in favor of sounds coming from vicinity of the

wearer's mouth and against sounds coming from elsewhere. In the DSP, digitized samples of the microphone outputs are processed to filter out airflow noise and to eliminate feedback from the loudspeakers to the microphones. The resulting conditioned version of the wearer's speech signal is sent to the transceiver.

This work was done by Marc A. Seibert of Glenn Research Center and Anthony J. Cullotta of Analex Corp. Further information is contained in a TSP (see page 1).

Inquiries concerning rights for the commercial use of this invention should be addressed to NASA Glenn Research Center, Innovative Partnerships Office, Attn: Steve Fedor, Mail Stop 4-8, 21000 Brookpark Road, Cleveland, Ohio 44135. Refer to LEW-17736-1.



The **Noise-Canceling Audio System** processes microphone outputs to maximize sensitivity to the wearer's speech, suppress feedback from loudspeakers to microphones, and filter out noise.

Program Analyzes Spacecraft/Ground Radio Links

NASA's Jet Propulsion Laboratory, Pasadena, California

A versatile computer program analyzes the link-design control table necessary for designing the telecommunication subsystem of a spacecraft in orbit around the Earth or on a deep-space mission. The program helps to calculate all the important parameter values for spacecraft-to-ground telemetry links and ground-to-spacecraft command links. The program also enables the design of turn-around ranging and one-way ranging links, which are very useful for determining the positions of spacecraft and for satisfying various other operational

needs. The user can specify several aspects of spacecraft telecommunication-subsystem design, including the nature of the antenna (paraboloidal reflector, patch, dipole, etc.), the power-amplifier rating, and the link data rate.

The program enables the use of comparative design procedures and includes an extensive database on the capabilities, attributes, and costs of commercially available telecommunications equipment. Hence, the program can also perform cost analyses. The software includes an extensive ground-station

database, so that link design can be carried out using different ground stations in a comparative process in an effort to select the best design. The output of the program is in the form of graphs as well as numbers.

This program was written by Faiza Lansing and Anil Kantak of Caltech for NASA's Jet Propulsion Laboratory. Further information is contained in a TSP (see page 1).

This software is available for commercial licensing. Please contact Karina Edmonds of the California Institute of Technology at (626) 395-2322. Refer to NPO-40442.

Two-Way Communication Using RFID Equipment and Techniques

Dynamic data could be exchanged, in addition to conventional static RFID data.

NASA's Jet Propulsion Laboratory, Pasadena, California

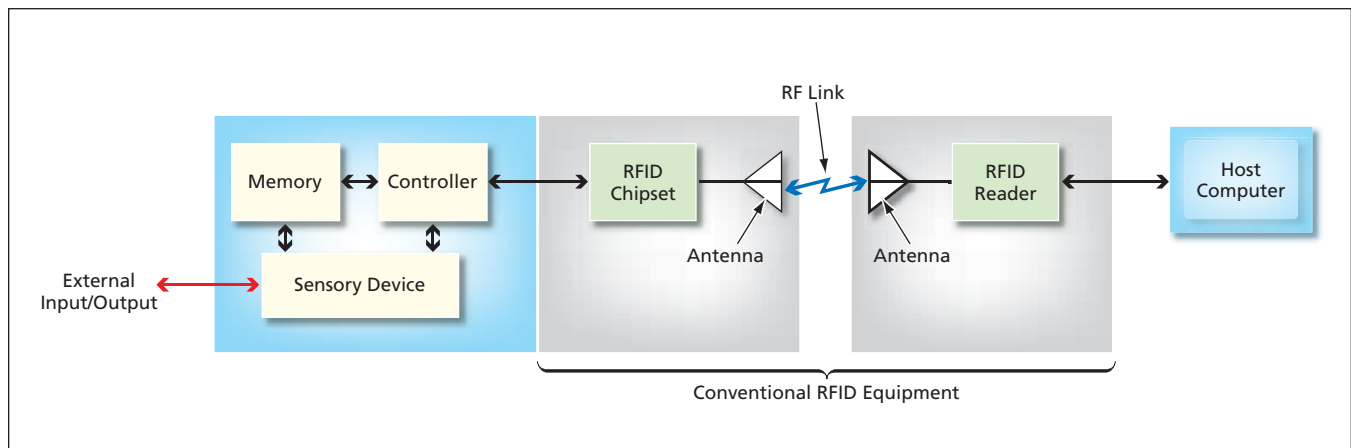
Equipment and techniques used in radio-frequency identification (RFID) would be extended, according to a proposal, to enable short-range, two-way communication between electronic products and host computers. In one example of a typical contemplated application, the purpose of the short-range radio communication would be to transfer image data from a user's digital still or video camera to the user's computer for recording and/or processing. The concept is also applicable to consumer electronic products other than digital cameras (for example, cellular telephones, portable computers, or motion sensors in alarm systems), and to a variety of industrial and scientific sensors and other devices that generate data.

Until now, RFID has been used to exchange small amounts of mostly static information for identifying and tracking assets. Information pertaining to an asset (typically, an object in inventory to be tracked) is contained in miniature electronic circuitry in an RFID tag attached to the object. Conventional RFID equipment and techniques enable a host computer to read data from and, in some cases, to write data to, RFID tags, but they do not enable such additional functions as sending commands to, or retrieving possibly large quantities of dynamic data from, RFID-tagged devices. The proposal would enable such additional functions.

The figure schematically depicts an implementation of the proposal for a

sensory device (e.g., a digital camera) that includes circuitry that converts sensory information to digital data. In addition to the basic sensory device, there would be a controller and a memory that would store the sensor data and/or data from the controller. The device would also be equipped with a conventional RFID chipset and antenna, which would communicate with a host computer via an RFID reader.

The controller would function partly as a communication interface, implementing two-way communication protocols at all levels (including RFID if needed) between the sensory device and the memory and between the host computer and the memory. The controller would perform power



An RFID System Extended as Proposed would enable a host computer to control a sensory device and retrieve data stored in the memory of that device.

management and other tasks essential to operation, and would encrypt data if necessary.

The RFID chipset would handle RFID communications (including implementing RFID protocols in cooperation with the controller). As in ordinary RFID tags, the RFID chipset would accept RF power received via the antenna, convert the RF power to DC power, and distribute the power both within itself and to any other circuitry as needed. The RFID chipset would interact with the controller to pass data from the sen-

sor memory to the host computer and/or to pass commands from the host computer.

The host computer would control the RFID reader. The host computer would contain application software and/or firmware that would enable the user to communicate with the sensory device and process data received from the sensory device.

This work was done by Thomas Jedry and Eric Archer of Caltech for NASA's Jet Propulsion Laboratory. Further information is contained in a TSP (see page 1).

In accordance with Public Law 96-517, the contractor has elected to retain title to this invention. Inquiries concerning rights for its commercial use should be addressed to:

*Innovative Technology Assets Management
JPL*

*Mail Stop 202-233
4800 Oak Grove Drive
Pasadena, CA 91109-8099
(818) 354-2240*

E-mail: iaoffice@jpl.nasa.gov

Refer to NPO-43144, volume and number of this NASA Tech Briefs issue, and the page number.

⚙️ Six-Message Electromechanical Display System

This system would overcome the three-message limit of prior such systems.

Marshall Space Flight Center, Alabama

A proposed electromechanical display system would be capable of presenting as many as six distinct messages. This system would be a more capable and more complex successor to the proposed system reported in "Four-Message Electromechanical Display System" (MFS-31368), *NASA Tech Briefs*, Vol. 24, No. 4 (April 2000), page 32. In contrast to the now-proposed six-message system and the previously proposed four-

message system, a typical conventional electromechanical display system is limited to three messages.

The three-message limit arises as follows: A typical electromechanical display system contains display elements with multiple flat faces that are rotated into view to present a message. Each display element can present, for example, an alphanumeric character or part of an image. If the display elements have flat

faces, then the number of messages is limited to three because three is the maximum number of sides of a polygon that can be placed contiguously with other, identical polygons along a common baseline and that can be rotated without interfering with an adjacent polygon.

In the proposed system (see Figure 1), each display element would include a cylinder having a regular hexagonal cross section. The adjacent

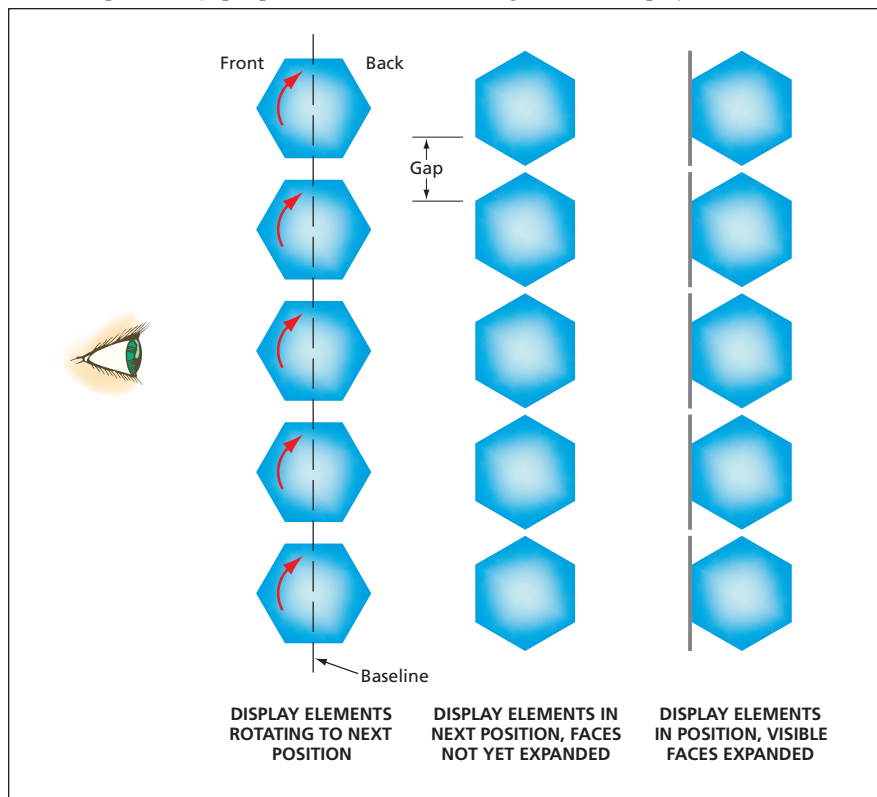


Figure 1. **Adjacent Hexagonal Cylinders** would be rotated to present any of six messages to viewers looking at the front side.

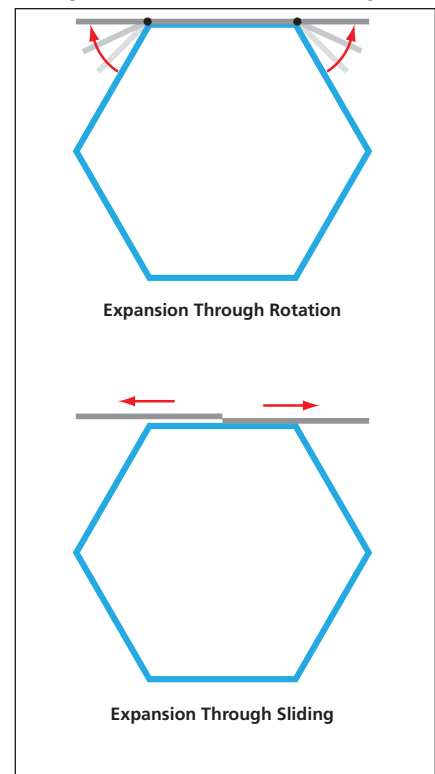


Figure 2. The **Visible Face of Each Hexagonal Cylinder** would effectively be expanded by rotation or sliding of panels.

elements would be positioned along a baseline with just enough room that each element could rotate without interfering with an adjacent element. As in the systems mentioned above, each face of each element would represent a portion of a message. Each element could be rotated to one of six equally spaced angular positions to present the desired portion of one of six messages. However, unlike in prior systems, merely orienting the desired

faces to form a flat surface visible to intended viewers would not suffice to present the message because there would be large gaps between the faces of the aligned hexagons.

To enable filling of the gaps between the visible aligned faces of adjacent hexagons, the affected portions of the messages would be placed on panels that would be rotated or slid to effectively expand the visible faces to fill or nearly fill the gaps (see Figure 2). After presenta-

tion of a message, panels would be retracted, restoring the hexagonal outlines to enable rotation of the elements to display the next message. Optionally, panels on both the front and the back of the display could be extended simultaneously to present different front and back messages.

This work was done by Richard T. Howard of Marshall Space Flight Center. Further information is contained in a TSP (see page 1). Refer to MFS-31576-1.



Scanning Terahertz Heterodyne Imaging Systems

These systems could reveal a wealth of information on biological and material specimens.

NASA's Jet Propulsion Laboratory, Pasadena, California

Scanning terahertz heterodyne imaging systems are now at an early stage of development. They were recently conceived as means of probing biological specimens and samples of materials to obtain information complementary to that obtainable from imaging systems that utilize other parts of the electromagnetic spectrum (e.g., visible light or x rays). Emerging applications for scanning terahertz heterodyne imaging systems include studies of terahertz contrast mechanisms in biological samples, pump-probe excitation of phonon modes in liquids and solids, studies of effects of terahertz irradiance on functions and forms of living cells, and studies of spectral signatures indicative of binding and structures of protein molecules.

Scanning terahertz heterodyne imaging systems using continuous-wave (CW) radiation offer the wide dynamic ranges and high signal-to-noise ratios characteristic of narrow-band high-spectral-resolution systems. As such, they also invite comparison with other terahertz imaging systems that utilize short-pulse time-domain spectroscopy (TDS), which is extremely powerful as a diagnostic technique but typically involves limitations in dynamic range and spectral resolution. One especially notable result of these differences is that in wet tissues, terahertz TDS systems are limited to penetration depths of the order of microns, while terahertz heterodyne systems can reach depths of the order of millimeters. Because the capabilities afforded by the terahertz heterodyne concept are partly complementary to those afforded by the terahertz short-pulse TDS concept, imaging systems based on these concepts could be used as complements to each other to obtain more information than could be obtained by use of either system alone.

In a basic scanning terahertz heterodyne imaging system, (see Figure 1) two far-infrared lasers generate beams denoted the local-oscillator (LO) and signal that differ in frequency by an amount, denoted the intermediate fre-

quency (IF), chosen to suit the application. The LO beam is sent directly to a mixer as one of two inputs. The signal beam is focused to a spot on or in the specimen. After transmission through or reflection from the specimen, the beams

are focused to a spot on a terahertz mixer, which extracts the IF outputs. The specimen is mounted on a translation stage, by means of which the focal spot is scanned across the specimen to build up an image.

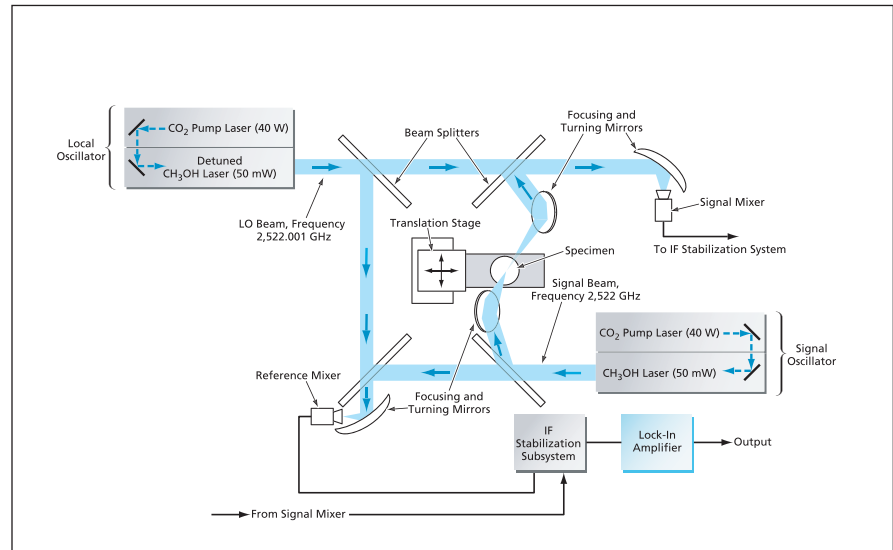


Figure 1. This Scanning Terahertz Heterodyne Imaging System incorporates an IF stabilization subsystem. This system is capable of a dynamic range of 10^9 , a penetration depth of 5 mm, a stability of 0.1 dB, and a resolution of 0.4 mm. The image-acquisition speed — about 30 pixels per second — is limited by the speed of the translation stage.

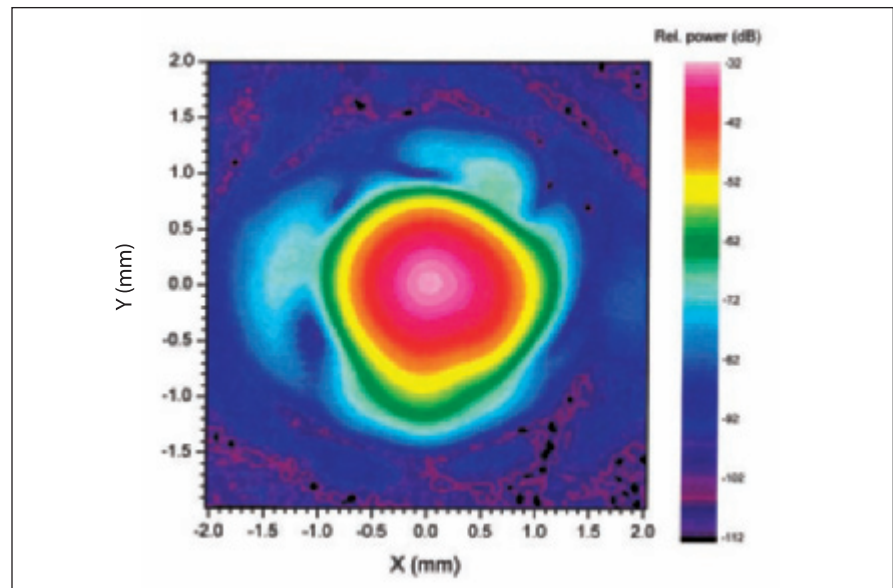


Figure 2. A 2.5-THz Laser Beam is imaged through a 150-micrometer diameter pin hole. Noise floor is -100 dB below peak detection level (0 dB).

The performance of the basic scanning terahertz heterodyne imaging system is limited by a number of factors, the most prominent one being frequency instability of the lasers. The figure depicts a more complex prototype system that incorporates an IF stabilization subsystem that increases the achievable frequency stability and dynamic range. This system utilizes two mixers denoted the reference and signal mixers, and the signal from each laser is split into two beams denoted the reference and signal beams. One of the lasers is slightly detuned so that their frequencies differ by an IF between 1 and 3 MHz. The IF outputs of the two mixers are equal in frequency; however, they differ in amplitude and phase because of the loss and phase shift suffered by the signal beam that passes through the

specimen and impinges on the signal mixer.

The IF output of the signal mixer becomes one of two inputs to a third mixer that is part of the IF stabilization subsystem. In a fourth mixer that is also part of the IF stabilization subsystem, the IF output of the reference mixer is mixed with a stable 14.6-MHz oscillator signal, and the resulting signal becomes the other input to the third mixer. The output of the third mixer and thus the output of the IF stabilization subsystem is a signal that has a stable frequency of 14.6 MHz but exhibits variations in amplitude and phase according to the loss and phase shift of the signal beam passing through the specimen. An improved system with an IF of 24 GHz has now been completed with a dynamic range of 100 dB

(Figure 2), 100 pixels/second, and penetration of 25 mm.

This work was done by Peter Siegel and Robert Dengler of Caltech for NASA's Jet Propulsion Laboratory. Further information is contained in a TSP (see page 1).

In accordance with Public Law 96-517, the contractor has elected to retain title to this invention. Inquiries concerning rights for its commercial use should be addressed to:

*Innovative Technology Assets Management
JPL*

Mail Stop 202-233

4800 Oak Grove Drive

Pasadena, CA 91109-8099

(818) 354-2240

E-mail: iaoffice@jpl.nasa.gov

Refer to NPO-40474, volume and number of this NASA Tech Briefs issue, and the page number.

Master Clock and Time-Signal-Distribution System

This system has a modular, flexible architecture and is user-friendly.

NASA's Jet Propulsion Laboratory, Pasadena, California

A timing system comprising an electronic master clock and a subsystem for distributing time signals from the master clock to end users is undergoing development to satisfy anticipated timing requirements of NASA's Deep Space Network (DSN) for the next 20 to 30 years. The developmental system is intended to supplant the aging DSN frequency and timing subsystem (FTS), which, while historically reliable, is complex, has limited distribution capacity and has become increasingly difficult to operate and sustain. This system has a modular, flexible, expandable architecture that is easier to operate and maintain than the present FTS. Replicas of this system could be useful in laboratories and other facilities in which there are stringent timing requirements that could include requirements to distribute precise time signals over long distances.

The system [to be installed in each Deep Space Communications Complex (DSCC) in the original DSN application] includes three major hardware assemblies interconnected by an infrastructure of fiber-optic cables (see figure). One major hardware assembly is the master clock assembly (MCA), wherein time signals are generated in synchronism with a 100-MHz reference signal from an atomic frequency standard, denoted the "online" standard.

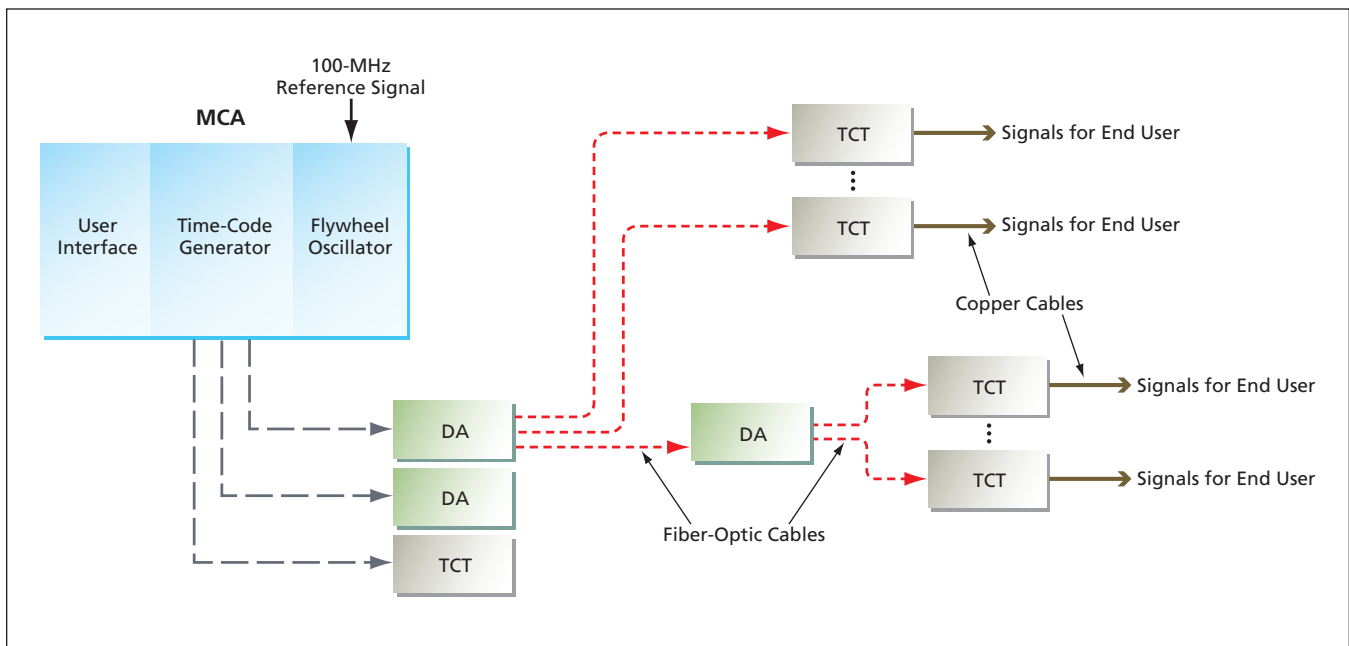
The MCA is set to Universal Coordinated Time and generates a system time code (STC) for distribution of time-of-day and timing-rate information to the entire DSCC. The STC is sent, via fiber-optic cables, to a distribution assembly (DA). The DA contains 10 distribution modules (DMs), each of which reconstitutes the STC and transmits the signal, either to a second-stage DA for additional fan-out or to a time-code translator (TCT), which serves as a timing reference interface for an end user. The TCT compensates for transmission delays from the MCA and can generate a variety of time codes and pulse rates as required.

The MCA, the DAs, and the TCTs reside in standardized chassis that are hot-swappable and include dual redundant power supplies. The MCA and DA chassis are identical; the TCT chassis are different and match those of the TCTs of the FTS. The back of each TCT can accommodate four plug-in modules to provide different time-code and pulse rate outputs.

For high reliability, the system includes, from the perspective of each end user, two flywheel oscillators. One flywheel oscillator is part of the MCA. The main purpose of this flywheel oscillator is to maintain MCA time in the event of loss or interruption of the reference sig-

nal from the online standard. While the timing performance slowly deteriorates in the absence of the reference signal, the complex remains operational until the reference signal can be restored. A second flywheel oscillator is part of each TCT. This oscillator enables the TCT to continue to generate time-code and pulse-rate outputs in the event of interruption of time signals anywhere in the distribution infrastructure. The TCT flywheel oscillator is allowed to run for a holdover interval up to 12 hours — more than enough time for diagnosis and repair.

This system is designed to be user-friendly, requiring minimal expertise and minimal human intervention for clock setup and diagnosis of faults. In the original DSN application, operators already have an overabundance of status and fault information to analyze. In this system, the only status or fault information provided to operators is that which facilitates isolation of a failure to the module level. Local alarm indications in a TCT, visible as lighted front-panel light-emitting diodes (LEDs), are summed together and communicated back to the applicable DA by simply blanking one pulse of a 1-pulse-per-second monitor return signal. A missing-pulse detector circuit in each DM in each DA responds to a



The **Timing System** consists of hardware modules interconnected by fiber-optic cables. This block diagram is a highly simplified representation: The real system has a more complex fan-out, with more modules, cables, and end users.

blanked pulse by turning on an LED in the DM. Each DA chassis contains one alarm representing the summed alarms of all 10 of its DMs. This alarm is passed further back up the hierarchy or collected by a status summary monitor

computer visible to operators. With modularity and simple “go/no-go” monitoring and alarm information, operators can maintain operations with little understanding of the nuances of the precise timing system.

This work was done by Robert Tjoelker, Malcolm Calhoun, Paul Kuhnle, Richard Sydnor, and John Lauf of Caltech for NASA's Jet Propulsion Laboratory. Further information is contained in a TSP (see page 1). NPO-40851

Synchronous Phase-Resolving Flash Range Imaging

Complete range images are generated, without scanning, at a video frame rate.

NASA's Jet Propulsion Laboratory, Pasadena, California

The figure is a simplified diagram of an apparatus, now undergoing development, for range imaging based on measurement of the round-trip phase delay of a pulsed laser beam. Variants of this apparatus could be used to provide range information needed for navigation of autonomous robotic ground vehicles and robotic aircraft, and for navigation and aiming in numerous military applications.

The apparatus would operate in a staring mode. A pulsed laser would illuminate a target. Laser light reflected from the target would be imaged on a very-large-scale integrated (VLSI)-circuit image detector, each pixel of which would contain a photodetector and a phase-measuring circuit. The round-trip travel time for the reflected laser light incident on each pixel, and thus the distance to the portion of the target imaged in that pixel, would be measured in terms of the phase difference between

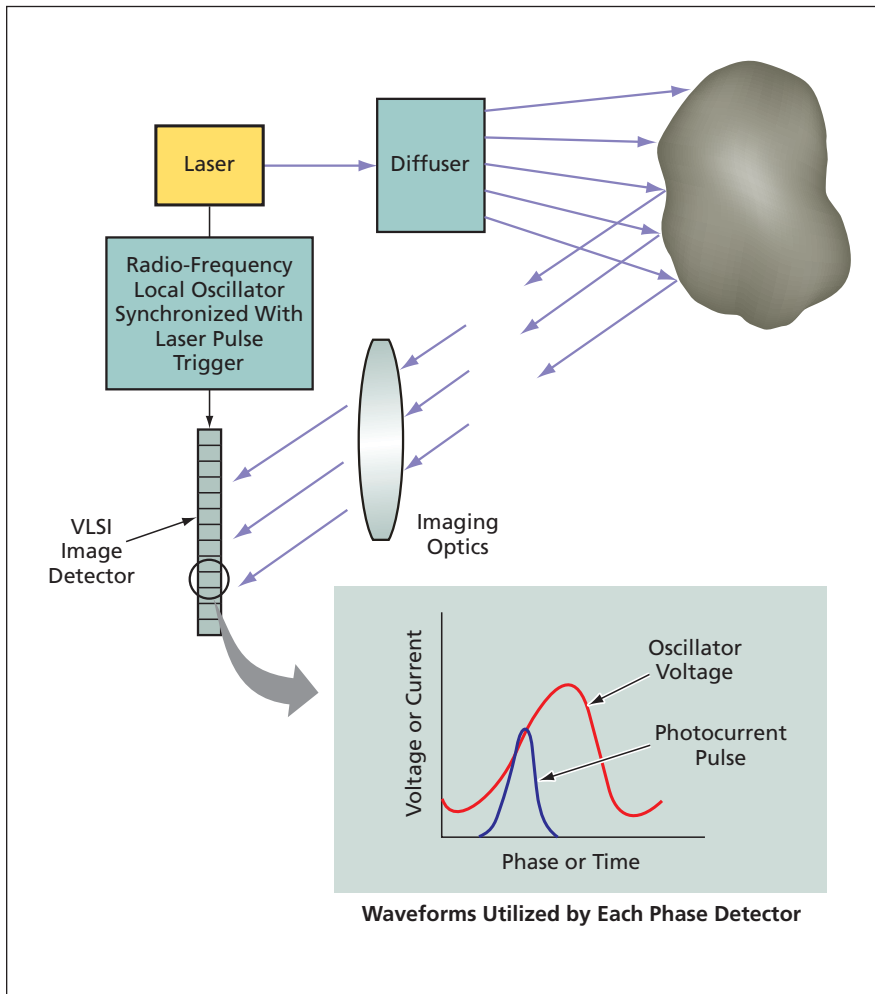
(1) the photodetector output pulse and (2) a local-oscillator signal that would have a frequency between 10 and 20 MHz and that would be synchronized with the laser-pulse-triggering signal.

This apparatus offers several advantages over prior laser range imagers (essentially, scanning lidar systems based on explicit measurement of round-trip pulse travel times). A typical scanning lidar system consumes tens of watts of power, must be large because of the need for complex optics and mechanical scanning, and must include a clock running at a frequency of the order of a gigahertz. Moreover, because of the need for mechanical scanning to build up a range image, it is not possible to achieve an update rate (frame rate) sufficient for most applications.

In contrast, because of its staring mode of operation, the developmental apparatus could utilize simpler optics and would contain no moving parts. Be-

cause of the elimination of mechanical scanning and the use of VLSI circuitry, the power demand of this apparatus would be only about 100 mW. Moreover, because a complete range image could be constructed for each successive laser pulse, it would be possible to achieve an update rate, greater than the standard video frame rate of 30 Hz, that would be sufficient for most robotic applications. It has been estimated that the apparatus could provide a range resolution of 1 cm. The maximum range of the apparatus would depend on the details of the design and the specific application: for example, on the basis of the minimum detectable photocurrent density, the maximum range would be about 1 km for a 15°-wide field of view or about 100 m for a 60°-wide field of view.

A prototype of the phase-measuring VLSI image detector has been demonstrated. In each pixel, the output of the photodiode and the local-oscillator sig-



In this Lidar Range-Imaging System voltage-to-phase converter circuits in each pixel that would be used to measure the phase of the lidar return pulse relative to the phase of a local-oscillator signal synchronized with the laser pulse.

nal are fed as inputs to a current-mirror circuit to obtain output currents proportional to the value of the local-oscillator sinusoid at the time of return of the laser pulse. In each of several phase-detector circuits, one of the current-mirror output currents is integrated in a capacitor to obtain a low-noise voltage indicative of the phase difference. This design enables accurate measurement of the phase difference because it is possible to measure voltage very accurately (to within microvolts) in VLSI circuits. The use of several phase detectors, each excited with a differently delayed replica of the local oscillator signal, makes it possible to measure the target distance accurately in the presence of unknown background illumination, unknown target albedo, and full-cycle phase ambiguities.

This work was done by Bedabrata Pain and Bruce Hancock of Caltech for NASA's Jet Propulsion Laboratory. Further information is contained in a TSP (see page 1).

In accordance with Public Law 96-517, the contractor has elected to retain title to this invention. Inquiries concerning rights for its commercial use should be addressed to:

*Innovative Technology Assets Management
JPL*

*Mail Stop 202-233
4800 Oak Grove Drive
Pasadena, CA 91109-8099
(818) 354-2240*

E-mail: iaoffice@jpl.nasa.gov

Refer to NPO-40811, volume and number of this NASA Tech Briefs issue, and the page number.

Integrated Radial Probe Transition From MMIC to Waveguide

Packaging based on wire bonding would be supplanted by monolithic integration.

NASA's Jet Propulsion Laboratory, Pasadena, California

A radial probe transition between a monolithic microwave integrated circuit (MMIC) and a waveguide has been designed for operation at frequency of 340 GHz and to be fabricated as part of a monolithic unit that includes the MMIC. Integrated radial probe transitions like this one are expected to be essential components of future MMIC amplifiers operating at frequencies above 200 GHz. While MMIC amplifiers for this frequency range have not yet been widely used because they have only recently been developed, there are numerous potential applications for them — especially in scientific instruments, test equipment, radar, and millimeter-wave

imaging systems for detecting hidden weapons.

One difficult problem in designing and fabricating MMIC amplifiers for frequencies greater than 200 GHz is that of packaging the MMICs for use as parts of instruments or for connection with test equipment. To package an MMIC for use or testing, it is necessary to mount the MMIC in a waveguide package, wherein the cross-sectional waveguide dimensions are typically of the order of a few hundred microns. Typically, in an MMIC/waveguide module for a microwave frequency well below 200 GHz, electromagnetic coupling between the MMIC and the wave-

guides is effected by use of a microstrip-to-waveguide transition that is (1) fabricated on a dielectric [alumina or poly(tetrafluoroethylene)] substrate separate from the MMIC and (2) wire-bonded to the MMIC chip. In the frequency range above 200 GHz, wire bonding becomes lossy and problematic, because the dimensions of the wire bonds are large fractions of a wavelength. In addition, fabrication of the transition is difficult at the small required thickness [typically of the order of 1 mil (25.4 μm)] of the dielectric substrate. The present design promises to overcome the disadvantages of the separate substrate/wire-bonding approach.

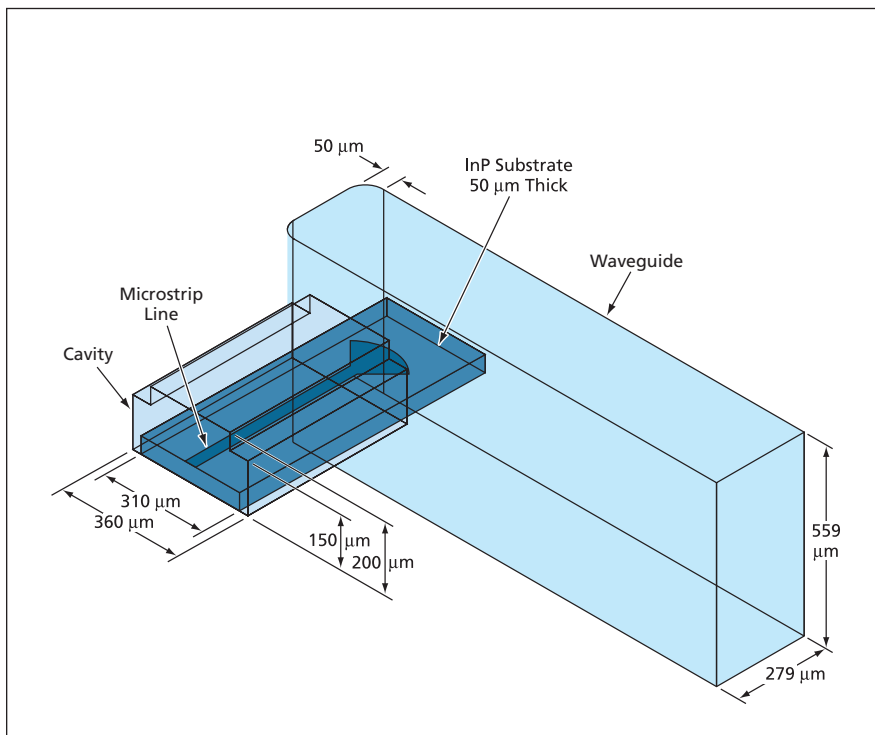


Figure 1. The **Integrated Radial Probe Transition** would couple 340-GHz electromagnetic radiation from an MMIC (not shown) on the InP substrate to the waveguide.

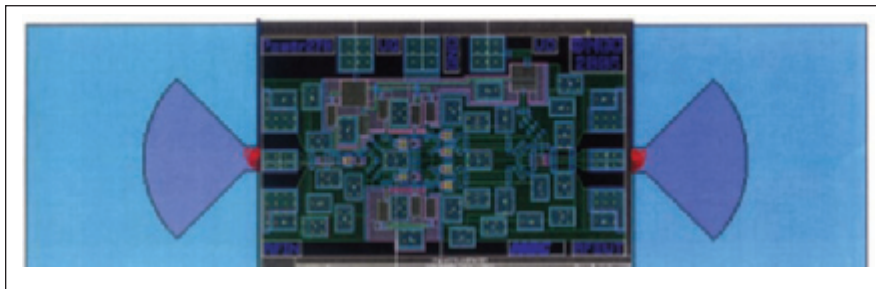


Figure 2. This is an Example Plan View of a 340-GHz MMIC amplifier chip that would incorporate radial probe transitions like that of Figure 1 at both ends. Backside metal would be removed in the probe areas.

The radial probe design could readily be adapted to integration with an MMIC amplifier because it provides for the fabrication of the transition on a substrate of the same material (InP), width (310 μm), and thickness (50 μm) typical of substrates of MMICs that can operate above 300 GHz. The figure depicts the basic geometric features of the design. The conductive part of the transition would be deposited on the InP substrate. The transition (and the rest of the MMIC chip if the transition were integrated with the MMIC) would reside in a metal cavity 360 μm wide having a stepped vertical dimension of total height 200 μm . The metal cavity would be essentially a reduced-cross-section lateral extension of the waveguide. The waveguide would be of a standard rectangular cross section, known in the art as WR2.2, having dimensions of 559 μm by 279 μm . There would be a 50- μm backshort between one vertical side of the metal cavity and the near end of the waveguide. The transition is designed to effect coupling between the microstrip mode of the MMIC chip and the transverse electric 10 (TE_{10}) electromagnetic mode of the waveguide. The choice of dimensions of the metal cavity and the waveguide is governed partly by the requirement that the cutoff frequency of the waveguide be less than the frequency of operation while the cutoff frequency of the transition's cavity must exceed the frequency of operation.

This work was done by Lorene Samoska and Goutam Chattopadhyay of Caltech for NASA's Jet Propulsion Laboratory. Further information is contained in a TSP (see page 1). NPO-43957

Bar-Code System for a Microbiological Laboratory

Time is saved and the incidence of errors is greatly reduced.

NASA's Jet Propulsion Laboratory, Pasadena, California

A bar-code system (see figure) has been assembled for a microbiological laboratory that must examine a large number of samples. The system includes a commercial bar-code reader, computer hardware and software components, plus custom-designed database software. The software generates a user-friendly, menu-driven interface.

Traditionally, microbiological samples have been labeled by hand, and recording of results of microbiological assays has entailed handwriting of bacterial-

colony counts in notebooks. This traditional approach is both time-consuming and susceptible to human error, especially when large numbers of samples are involved. By automating the routine aspects of tracking microbiological samples, recording data, and documentation of samples and results, the bar-code system saves time and greatly reduces the incidence of errors.

The bar-code system prints unique bar-code labels that can be easily affixed to test tubes and Petri dishes. During

sampling, a technician or microbiologist affixes the labels and uses a personal digital assistant (PDA) with a built-in bar-code scanner to scan the bar codes and record notes. After sampling, the data acquired by the bar-code scanner are downloaded to the bar-code-system database, and then a microbiologist assays the samples.

To record assay results, the microbiologist scans the bar-code label on each test tube or Petri dish and records the data specific to that sample container on



The **Bar-Code System Hardware** includes a personal computer, a desktop bar-code scanner (on the right by tubes and plates), and a PDA with a built-in bar-code scanner (left of the keyboard).

an interactive computer display in a location reserved for those specific data. Inasmuch as the database software is designed to display only the record that

corresponds to a given bar code, the possibility of accidentally recording data in the wrong place is eliminated (except, of course, for rare instances of computer error or errors in re-affixation of labels that have fallen off). In addition, because the microbiologist no longer needs to painstakingly find the correct place to enter data for each assay plate, the bar-code system accelerates the process of reading plates and recording data.

The bar-code system greatly simplifies the documentation of the sampling

process. During sampling, the note-taking capability of the PDA is complemented by the use of a digital camera: The sampling technician or microbiologist takes a picture of each sample and records the picture number (as assigned by the digital camera) in the PDA. Once the data and pictures are downloaded to the database, only a few mouse clicks are necessary to generate a two-column report that displays the pictures in one column and lists the corresponding samples and pertinent information in the other column. In addition, the bar-code system automatically generates a report of assay results. The data in the report can be exported to a spreadsheet for analysis.

This work was done by Jennifer Law and Larry Kirschner of Caltech for NASA's Jet Propulsion Laboratory. Further information is contained in a TSP (see page 1). NPO-30815

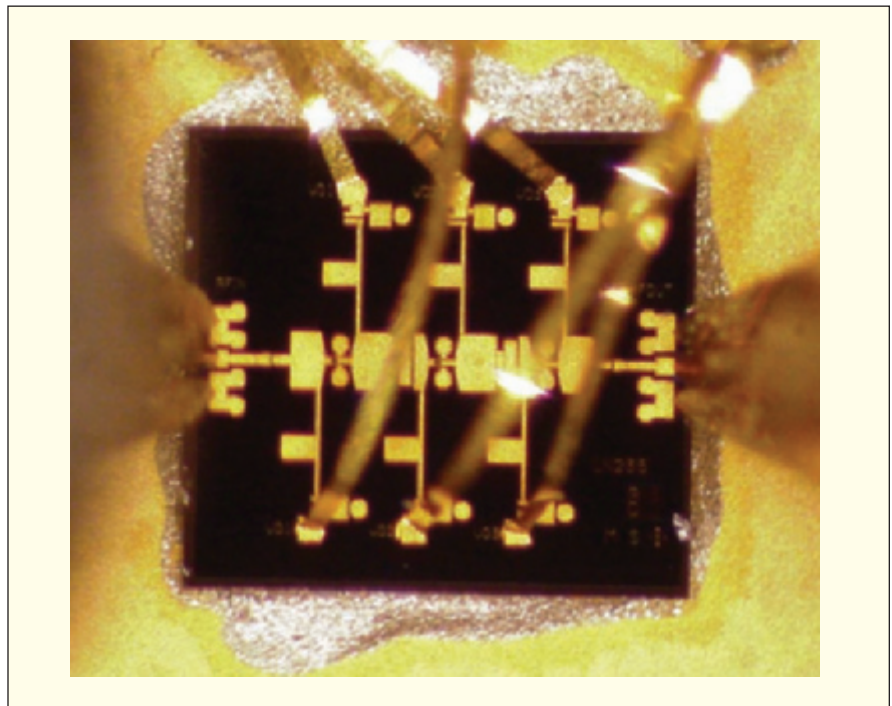
MMIC Amplifier Produces Gain of 10 dB at 235 GHz

This is the fastest MMIC amplifier reported to date.

NASA's Jet Propulsion Laboratory, Pasadena, California

The first solid-state amplifier capable of producing gain at a frequency >215 GHz has been demonstrated. This amplifier is an intermediate product of a continuing effort to develop amplifiers having the frequency and gain characteristics needed for a forthcoming generation of remote-sensing instruments for detecting water vapor and possibly other atmospheric constituents. There are also other potential uses for such amplifiers in wide-band communications, automotive radar, and millimeter-wave imaging for inspecting contents of opaque containers.

This amplifier was fabricated as a monolithic microwave integrated-circuit (MMIC) chip containing InP high-electron-mobility transistors (HEMTs) of 0.07- μm gate length on a 50- μm -thick InP substrate. The passive components on the chip are of the microstrip type and were designed by use of advanced electromagnetic-behavior-simulation software. The amplifier contains three stages of HEMTs with matching networks that comprise microstrip transmission lines and metal/insulator/metal capacitors. Bias is supplied via transmission-line networks with bypass capacitors on the gate and drain sides of the HEMTs.



The **MMIC Amplifier** described in the text is shown mounted for testing with custom wafer probes for testing at 220 to 325 GHz.

The performance of the amplifier was measured by use of the instrumentation system described in "Equipment for On-Wafer Testing From 220 to 325 GHz"

(NPO-40955), *NASA Tech Briefs*, Vol. 30, No. 1 (January 2006), page 38. This instrumentation system, equivalent to a two-port vector network analyzer, was

equipped with custom wafer probes (see figure) designed for the noted frequency band, which is that of WR-3 waveguides [waveguides having a standard rectangular cross section of 0.0340 by 0.0170 in. (0.8636 by 0.4318 mm)].

Among other things, the measurements showed a peak gain of 10 dB at a frequency of 235 GHz.

This work was done by Douglas Dawson, King Man Fung, Karen Lee, Lorene Samoska, Mary Wells, Todd Gaier, and

Pekka Kangaslahti of Caltech; and Ronald Grundbacher, Richard Lai, Rohit Raja, and Po-Hsin Liu of NGST for NASA's Jet Propulsion Laboratory. Further information is contained in a TSP (see page 1). NPO-42202

Mapping Nearby Terrain in 3D by Use of a Grid of Laser Spots

A relatively simple system would utilize triangulation.

NASA's Jet Propulsion Laboratory, Pasadena, California

A proposed optoelectronic system, to be mounted aboard an exploratory robotic vehicle, would be used to generate a three-dimensional (3D) map of nearby terrain and obstacles for purposes of navigating the vehicle across the terrain and avoiding the obstacles. Like some other systems that have been, variously, developed and proposed to perform similar functions, this system would include (1) a light source that would project a known pattern of bright spots onto the terrain, (2) an electronic camera

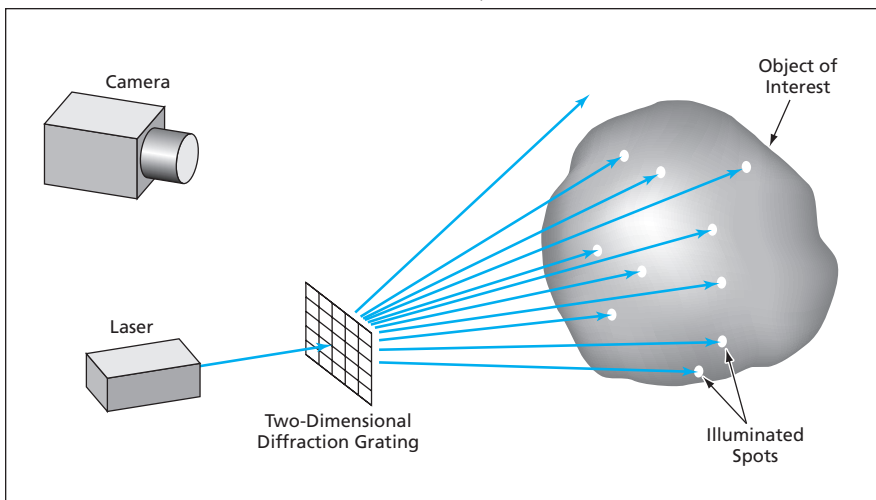
that would be laterally offset from the light source by a known baseline distance, (3) circuitry to digitize the output of the camera during imaging of the light spots, and (4) a computer that would calculate the 3D coordinates of the illuminated spots from their positions in the images by triangulation.

The difference between this system and the other systems would lie in the details of implementation. In this system, the illumination would be provided by a laser. The beam from the laser

would pass through a two-dimensional diffraction grating, which would divide the beam into multiple beams propagating in different, fixed, known directions (see figure). These beams would form a grid of bright spots on the nearby terrain and obstacles. The centroid of each bright spot in the image would be computed. For each such spot, the combination of (1) the centroid, (2) the known direction of the light beam that produced the spot, and (3) the known baseline would constitute sufficient information for calculating the 3D position of the spot.

Concentrating the illumination into spots, instead of into lines as in some other systems, would afford signal-to-noise ratios greater than those of such other systems and would thereby also enable this system to image terrain and obstacles out to greater distances. The laser could be pulsed to obtain momentary illumination much brighter than ambient illumination, and the camera could be synchronized with the laser to discriminate against ambient light between laser pulses.

This work was done by Curtis Padgett, Carl Liebe, Johnny Chang, and Kenneth Brown of Caltech for NASA's Jet Propulsion Laboratory. Further information is contained in a TSP (see page 1). NPO-40611



A Diffraction Grating Would Split a Laser Beam into multiple beams to project a grid of bright spots onto an object of interest. A camera offset from the laser and diffraction grating would capture an image of the illuminated spots. The 3D positions of the spots would be computed from their positions in the image by triangulation.

Digital Beam Deflectors Based Partly on Liquid Crystals

Laser beams are switched to different directions, without using solid moving parts.

John H. Glenn Research Center, Cleveland, Ohio

A digital beam deflector based partly on liquid crystals has been demonstrated as a prototype of a class of optical beam-steering devices that contain no mechanical actuators or solid moving parts. Such beam-steering devices could

be useful in a variety of applications, including free-space optical communications, switching in fiber-optic communications, general optical switching, and optical scanning. Liquid crystals are of special interest as active materials in

nonmechanical beam steerers and deflectors because of their structural flexibility, low operating voltages, and the relatively low costs of fabrication of devices that contain them. Recent advances in synthesis of liquid-crystal ma-

materials and design of the nematic-liquid-crystal cells have resulted in significant improvements in properties (e.g., short response times and birefringence) that are important for effective beam steering.

A beam deflector of this type is a multistage device. Each stage consists mainly of (1) a passive birefringent prism made of yttrium orthovanadate (YVO₄) [alternatively, it could be made of a uniaxial smectic A liquid crystal] and (2) a switchable polarization rotator in the form of a cell containing a twisted nematic liquid crystal. A linearly polarized laser beam that one seeks to deflect travels through the liquid-crystal cell on the way to the passive birefringent prism. If no voltage is applied across the cell (“off” state), passage through the cell changes the direction of polarization by

90°. If a suitable non-zero voltage is applied across the cell (“on” state), then the polarization direction remains unchanged after passage through the cell. Therefore, by virtue of birefringence, depending on which of the two selectable polarizations has been imparted to the beam by the liquid-crystal cell, the beam propagates through the crystal in either of two different directions.

If a beam deflector of this type contained N stages, then it would be possible to switch the input laser beam to any of 2^N different output directions through electrical switching of the liquid-crystal cells. The prototype device operates with an incident 633-nm-wavelength beam from a helium/neon laser. It contains 4 stages and, hence, can deflect the beam to any of $2^4 = 16$ output directions. In this case, the directions

are separated by increments of 8 milliradians. To obtain a relatively short response time (0.5 ms), the cells are made from so-called dual-frequency nematic liquid crystals and operated in a special addressing scheme that features amplitude- and frequency-modulated driving voltage.

This work was done by John J. Pouch and Felix A. Miranda of Glenn Research Center; Liubov Kreminska, Oleg Pishnyak, Andrii Golovin, and Oleg D. Lavrentovich of Kent State University; and Bruce K. Winker of Rockwell Scientific Company LLC. Further information is contained in a TSP (see page 1).

Inquiries concerning rights for the commercial use of this invention should be addressed to NASA Glenn Research Center, Innovative Partnerships Office, Attn: Steve Fedor, Mail Stop 4-8, 21000 Brookpark Road, Cleveland, Ohio 44135. Refer to LEW-17947-1.

Narrow-Band WGM Optical Filters With Tunable FSRs

Microwave signals generated by optoelectronic oscillators can be tuned.

NASA's Jet Propulsion Laboratory, Pasadena, California

Optical resonators of the whispering-gallery-mode (WGM) type featuring DC-tunable free spectral ranges (FSRs) have been demonstrated. Previously, the FSRs of WGM optical resonators were determined solely by the resonator geometries and materials: hence, the FSR of such a resonator could be tailored by design, but once the resonator was constructed, its FSR was fixed. By making the FSR tunable, one makes it possible to adjust, during operation, the frequency of a microwave signal generated by an optoelectronic oscillator in which an WGM optical resonator is utilized as a narrow-band filter.

Each tunable WGM resonator was made from a disk of lithium niobate, 2.6 mm in diameter and 120 μm thick. The edge of the disk was rounded by polishing to an approximately spherical surface. A ferroelectric-domain structure characterized by a set of rings concentric with the axis of the disk (see Figure 1) was created by means of a poling process in which a 1- μm -diameter electrode was dragged across the top surface of the disk in the concentric-ring pattern while applying a 2.5-kV bias between the electrode and a conductor in contact with the bottom surface of the disk. After the poling process, the top and bottom surfaces of the disk were

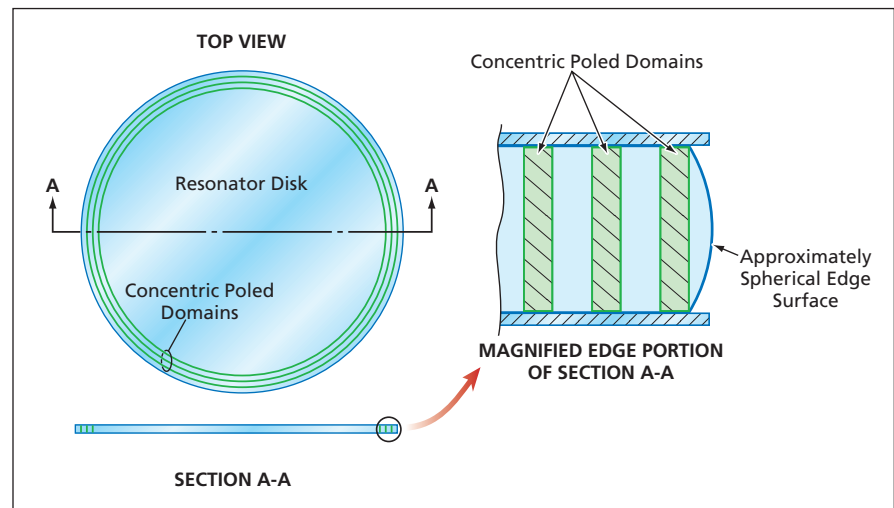


Figure 1. Concentric Poled Domains in a ferroelectric electro-optical resonator disk can be engineered to enable relative frequency shifting of adjacent radial resonator modes.

placed in contact with metal electrodes that, in turn, were connected to a regulated DC power supply that was variable from 0 to 150 V. When a DC bias electric field is applied in such a structure, the indices of refraction in the positively poled concentric rings and in the unflipped, negatively poled concentric regions change by different amounts.

The concentric-ring ferroelectric-domain structure of such a resonator can be engineered so that it overlaps with one or more radial resonator modes more than

it does with other, adjacent modes. As a result, when the indices of refraction change in response to DC bias, some modes shift in frequency by amounts that differ from those of adjacent modes; the difference in frequency shift amounts to the desired change in the FSR between the affected adjacent modes.

A test was performed on each tunable resonator to observe the absorption spectrum of the resonator and the changes in frequencies of adjacent modes of interest as the applied DC bias voltage was varied.

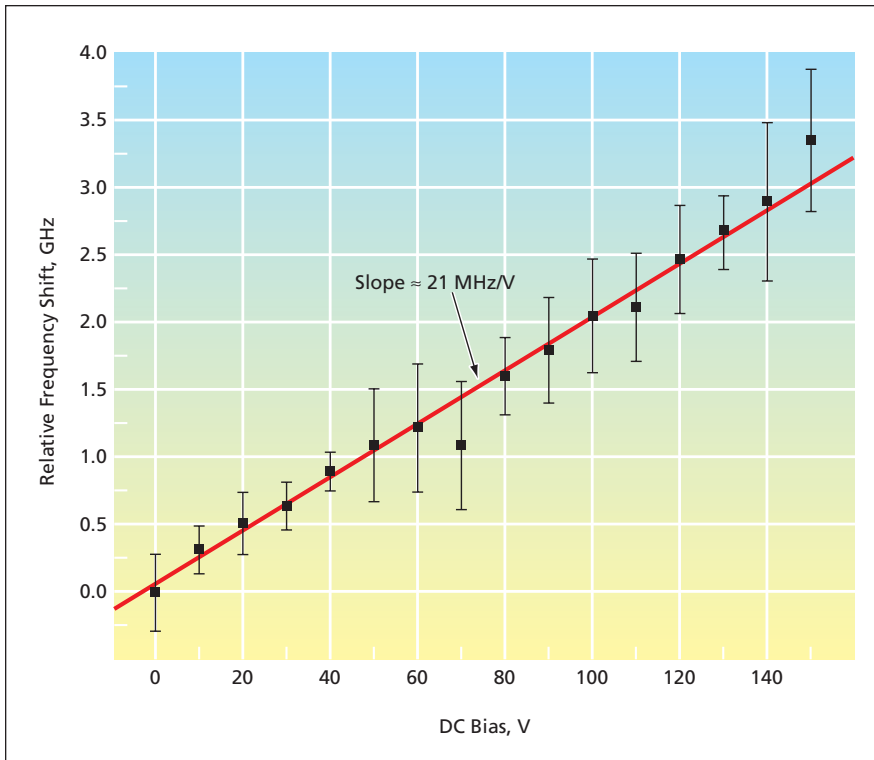


Figure 2. The **Relative Frequency Shift** between selected adjacent modes of an experimental resonator was found to vary with DC potential at a rate of about 21 MHz/V.

In this test, a probe optical beam having a nominal wavelength of 1.55 μm , scanned over a frequency range of 20 GHz, was coupled into the resonator through a diamond prism. Figure 2 presents some results of one such test, in which the frequency shift between two selected adjacent modes exhibited the desired variation with bias voltage.

This work was done by Makan Mohageg, Andrey Matsko, Anatoliy Savchenkov, Lute Maleki, Vladimir Iltchenko, and Dmitry Strekalov of Caltech for NASA's Jet Propulsion Laboratory. Further information is contained in a TSP (see page 1).

In accordance with Public Law 96-517, the contractor has elected to retain title to this invention. Inquiries concerning rights for its commercial use should be addressed to:

Innovative Technology Assets Management

JPL

Mail Stop 202-233

4800 Oak Grove Drive

Pasadena, CA 91109-8099

(818) 354-2240

E-mail: iaoffice@jpl.nasa.gov

Refer to NPO-41359, volume and number of this NASA Tech Briefs issue, and the page number.



Better Finite-Element Analysis of Composite Shell Structures

A computer program implements a finite-element-based method of predicting the deformations of thin aerospace structures made of isotropic materials or anisotropic fiber-reinforced composite materials. The technique and corresponding software are applicable to thin shell structures in general and are particularly useful for analysis of thin beam-like members having open cross-sections (e.g. I-beams and C-channels) in which significant warping can occur.

In many popular commercial packages that offer the two-dimensional finite elements option, inaccuracies arise from node offsets and overlapping of elements; in other formulations utilizing one-dimensional discretization, angles of twist tend to be overestimated. In the present formulation, a shell element that incorporates "floating" reference surfaces on which nodal points reside is developed. This element concept facilitates the formation of proper connections among elements and thereby eliminates the inaccuracies attributable to element-overlapping and nodal offsets in the other methods.

*This program was written by Gregory Clarke of Goddard Space Flight Center. Further information is contained in a TSP (see page 1).
GSC-14756-1*

Computing Spacecraft-Pointing Vectors for Limb Tracking

LMBTRK is a computer program that is used together with two software libraries known as ERHAND and HYBRRD to generate spacecraft-pointing vectors for limb-tracking maneuvers needed for experiments on propagation of radio signals through planetary atmospheres. LMBTRK determines, as a function of time, the direction in which one must point a ray (representing a radio beam) emitted by a spacecraft in order to make the ray pass through a

planetary atmosphere on its way to a receiving station at a known location. LMBTRK was written for Sun computers running the Solaris operating system and has been running on a cluster of such computers used in the Radio Science System of the Cassini Spacecraft mission.

This program was written by Nicole Rappaport and Essam Marouf of Caltech for NASA's Jet Propulsion Laboratory. Further information is contained in a TSP (see page 1).

This software is available for commercial licensing. Please contact Karina Edmonds of the California Institute of Technology at (626) 395-2322. Refer to NPO-40542.

Enhanced Master Controller Unit Tester

The Enhanced Master Controller Unit Tester (EMUT) software is a tool for development and testing of software for a master controller (MC) flight computer. The primary function of the EMUT software is to simulate interfaces between the MC computer and external analog and digital circuitry (including other computers) in a rack of equipment to be used in scientific experiments. The simulations span the range of nominal, off-nominal, and erroneous operational conditions, enabling the testing of MC software before all the equipment becomes available.

The EMUT software comprises a Win32-based set of three programs that run on different computers and are linked by Common Object Request Broker (CORBA) Ethernet communications. The main program, denoted the EMUT 1553 Application, generates a graphical user interface and is responsible for all communications via several MIL-STD-1553B data buses and for logging of output data. The second program, denoted the Analog Application, implements mathematical models of equipment (e.g., sensors and valves) and analog signals generated by the equipment and is responsible for all analog-signal communications with the MC. The third program, denoted the EMUT

Model Viewer, provides a graphical interface for viewing the statuses of the aforementioned models.

*This program was written by Patricia Benson, Yvette Johnson, and Brian Johnson of Marshall Space Flight Center; Philip Williams of Dynamic Concepts, Inc.; Geoffrey Burton of Madison Research Corp.; and Anthony McCoy of ERC. Further information is contained in a TSP (see page 1).
MFS-32172-1*

Rover Graphical Simulator

Rover Graphical Simulator (RGS) is a package of software that generates images of the motion of a wheeled robotic exploratory vehicle (rover) across terrain that includes obstacles and regions of varying traversability. The simulated rover moves autonomously, utilizing reasoning and decision-making capabilities of a fuzzy-logic navigation strategy to choose its path from an initial to a final state. RGS provides a graphical user interface for control and monitoring of simulations.

The numerically simulated motion is represented as discrete steps with a constant time interval between updates. At each simulation step, a dot is placed at the old rover position and a graphical symbol representing the rover is redrawn at the new, updated position. The effect is to leave a trail of dots depicting the path traversed by the rover, the distances between dots being proportional to the local speed. Obstacles and regions of low traversability are depicted as filled circles, with buffer zones around them indicated by enclosing circles. The simulated robot is equipped with onboard sensors that can detect regional terrain traversability and local obstacles out to specified ranges. RGS won the NASA Group Achievement Award in 2002.

This program was written by Bruce Bon and Homayoun Seraji of Caltech for NASA's Jet Propulsion Laboratory. Further information is contained in a TSP (see page 1).

This software is available for commercial licensing. Please contact Karina Edmonds of the California Institute of Technology at (626) 395-2322. Refer to NPO-35223.



Increasing Durability of Flame-Sprayed Strain Gauges

Low-oxygen heat treatments and internal platinum oxygen-diffusion barriers extend lifetimes.

John H. Glenn Research Center, Cleveland, Ohio

Thermally sprayed dielectric ceramic coatings are the primary means of attaching strain and temperature gauges to hot-section rotating parts of turbine engines. As hot-section temperatures increase, lifetimes of installed gauges decrease, and seldom exceed one hour above 2,000 °F (≈1,100 °C). Advanced engine components are expected to operate at temperatures approaching 2,200 °F (≈1,200 °C), and the required high-temperature lifetime is 10 hours minimum.

Typically, to enable a ceramic coating to adhere to the smooth surface of an engine component, a thermally sprayed NiCrAlY or NiCoCrAlY bond coat is applied to the smooth surface, thereby providing a textured surface to which

the ceramic coat can adhere. The main failure mechanism of this system is decohesion and/or delamination at the interface between the ceramic top coat and the bond coat, caused by oxidation of the bond coat and stresses from the mismatch between the coefficients of thermal expansion of the ceramic top coat and the metallic bond coat.

The approach taken to increase the high-temperature lifetime of a gauge attached to an engine component by the method described above involves (1) selective oxidation of the bond coat by means of a heat treatment in reduced oxygen partial pressure followed by (2) the application of a noble-metal diffusion barrier. In experiments to test this approach, heat treatments of NiCoCrAlY

bond coats were carried out in a tube furnace in which, in each case, the temperature was alternately (1) increased at a rate of 3 °C per minute and (2) held steady for one hour until the desired temperature was reached. The tube furnace was continuously purged with dry nitrogen gas. A final heat-treatment temperature range of 1,600 to 1,800 °F (871 to 982 °C) proved most beneficial.

Test coupons were made to enable evaluation of the cycle lives of various bond coats, including some made from the commercially available coating materials Praxair 171 (an NiCoCrAlY formulation) and Praxair 343 (an NiCrAlY formulation). Each test coupon included a base-metal coupon of Inconel™ 718 nickel alloy. One of the bond-coating materials to be tested was thermally sprayed on the metal, the coupon was subjected to the aforementioned heat treatment at reduced oxygen partial pressure, then a ceramic dielectric top-coat was thermally sprayed onto the bond coat. To provide a basis of comparison for evaluation of the relative merits of the various surface treatments and heat treatments, some of the NiCoCrAlY and NiCrAlY bond coats were incorporated into the coupons in the as-sprayed condition: that is, the affected coupons were not subjected to the heat treatment at reduced oxygen partial pressure.

Each coupon was mounted on an Inconel™ 718 nickel-alloy fixture and

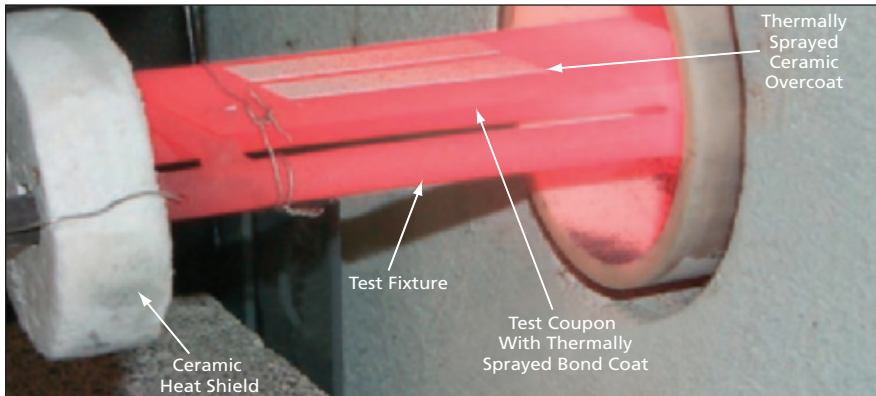


Figure 1. A Test Fixture is depicted here during removal from a horizontal tube furnace maintained at a temperature of 1,100 °C. A coupon is fastened to the fixture with platinum wire.

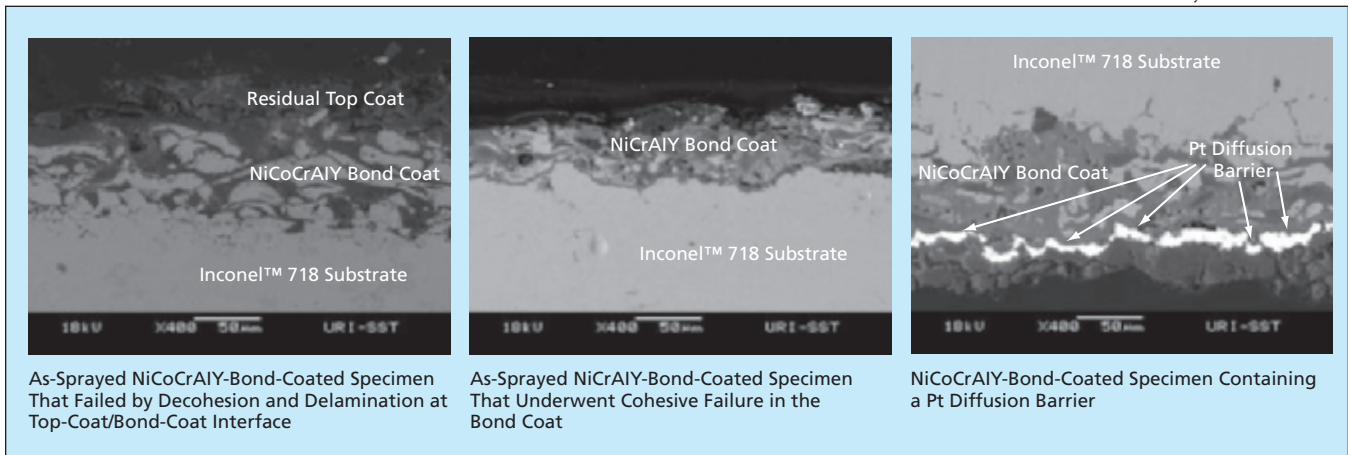


Figure 2. These Scanning Electron Micrographs of cross sections of representative coupons illustrate three different conditions described in the text.

placed in the tube furnace, wherein it was heated to 1,150 °C and held at this temperature for one hour. The test fixture was then retracted from the furnace (see Figure 1) and allowed to cool to 150 °C. The cooling process took approximately 5 to 6 minutes. Upon reaching 150 °C, the test fixture with the coupon was placed back in the furnace and reheated to 1,150 °C. The entire heating-and-cooling sequence was considered one cycle, and the lifetimes of the coupons were assessed on the basis of the numbers of cycles to failure.

The heat treatment of the NiCoCrAlY bond coats at reduced oxygen partial pressure yielded a significant increase in lifetimes: Coupons heat-treated to 1,750 °F (954 °C) at reduced oxygen partial pressure exhibited more than double the cycle lives of those containing as-sprayed NiCoCrAlY. This considerable increase in life can be attributed to the fact that selective oxidation of the aluminum and chromium in the bond coat yielded a graded interface. The heat treatment of the NiCrAlY bond coats yielded little or no increase in lifetimes.

The failure mechanisms of the coupons containing NiCoCrAlY bond coats differed from those of the coupons

containing the NiCrAlY bond coats: The NiCoCrAlY-bond-coated specimens failed by decohesion and/or delamination at the interfaces between the top and bond coats. The NiCrAlY-bond-coated specimens underwent cohesive failure within the bond coats. Evidence of failure by these mechanisms can be seen in the left and the middle part, respectively, of Figure 2.

In an effort to reduce the extent of internal oxidation in the bond coats, platinum and rhodium coats were employed as diffusion barriers. Initially, as-sprayed NiCoCrAlY-bond-coated coupons were coated with platinum to a thickness of 2 µm by physical vapor deposition (PVD). An example of a platinum diffusion barrier can be seen in the right part of Figure 2. The platinum-coated Inconel coupons were heat-treated to 1,800 °F (982 °C), then magnesium aluminate spinel top coats were thermally sprayed over the platinum coats. Rhodium diffusion barriers were applied to the surfaces of NiCoCrAlY-bond-coated coupons by pen electroplating. (Pen electroplating was investigated as a means of forming diffusion barriers because it is easy to perform and does not entail costly capital investment.)

The rhodium diffusion barriers yielded only a marginal increase in the lives of NiCoCrAlY-bond-coated coupons. However, platinum diffusion barriers applied by PVD in conjunction with reduced-oxygen-partial-pressure heat treatment yielded substantial increases in lifetimes. The platinum films were thick enough to constitute oxygen-diffusion barriers that slowed the growth of internal oxides by promoting the formation of alumina-rich scale at the interfaces between the top and bond coats. The best results achieved to date were realized by use of sputtered platinum diffusion barriers in conjunction with heat treatments to 1,800 °F (982 °C) at reduced oxygen partial pressures. This combination yielded a four-fold increase in the fatigue lives of NiCoCrAlY-bond-coated coupons.

This work was done by Otto J. Gregory and Markus A. Downey of the University of Rhode Island, and Steve Wnuk and Vince Wnuk of HPI Inc. for Glenn Research Center.

Inquiries concerning rights for the commercial use of this invention should be addressed to NASA Glenn Research Center, Innovative Partnerships Office, Attn: Steve Fedor, Mail Stop 4-8, 21000 Brookpark Road, Cleveland, Ohio 44135. Refer to LEW-17530-1.

Multifunctional, High-Temperature Nanocomposites

Electrical and thermal conductivities increase with proportions of nanotubes.

Langley Research Center, Hampton, Virginia

In experiments conducted as part of a continuing effort to incorporate multifunctionality into advanced composite materials, blends of multi-walled carbon nanotubes and a resin denoted “PETI-330” (wherein “PETI” is an abbreviation for “phenylethynyl-terminated imide”) were prepared, characterized, and fabricated into moldings. PETI-330 was selected as the matrix resin in these experiments because of its low melt viscosity (<10 poise at a temperature of 280 °C), excellent melt stability (lifetime >2 hours at 280 °C), and high temperature performance (>1,000 hours at 288 °C). The multi-walled carbon nanotubes (MWCNTs), obtained from the University of Kentucky, were selected because of their electrical and thermal conductivity and their small diameters. The purpose of these experiments was to determine the combination of thermal, electrical, and mechanical properties achievable while still maintaining melt

processability.

The PETI-330/MWCNT mixtures were prepared at concentrations ranging from 3 to 25 weight-percent of MWCNTs by dry mixing of the constituents in a ball mill using zirconia beads. The resulting powders were characterized for degree of mixing and thermal and rheological properties. The neat resin was found to have melt viscosity between 5 and 10 poise. At 280 °C and a fixed strain rate, the viscosity was found to increase with time. At this temperature, the phenylethynyl groups do not readily react and so no significant curing of the resin occurred. For MWCNT-filled samples, melt viscosity was reasonably steady at 280 °C and was greater in samples containing greater proportions of MWCNTs. The melt viscosity for 20 weight-percent of MWCNTs was found to be ≈28,000 poise, which is lower than the initial estimated allowable maximum value of 60,000 poise for injection mold-

ing. Hence, MWCNT loadings of as much as 20 percent were deemed to be suitable compositions for scale-up.

High-resolution scanning electron microscopy (HRSEM) showed the MWCNTs to be well dispersed in the polymer matrices, while high-resolution transmission electron microscopy shows splits in the walls of the MWCNTs but no catastrophic breakage of tubes. To further assess processing characteristics prior to scale-up, samples containing 10, 15, and 20 weight-percent of MWCNTs were processed through a laboratory melting extruder. HRSEM of the extruded fibers shows significant alignment of MWCNTs in the flow direction (see figure). For the samples containing 20 weight-percent of MWCNTs, difficulties were encountered during feeding, and the temperature of a rotor in the extruder rose to 245 °C because of buildup of frictional heat; this indicates that materials of this type having MWCNT concentra-

tions ≥ 20 weight-percent may not be melt-processable.

On the basis of the results from the foregoing characterizations, samples containing 10, 15, and 20 weight-percent of MWCNTs were scaled up to masses of ≈ 300 g and used to make specimens having dimensions of 10.2 by 15.2 by 0.32 cm. These specimens were molded by (1) injecting the mixtures, at temperatures between 260 and 280 °C, into a tool made of the low-thermal-expansion alloy Invar[®] and then (2) curing for 1 hour at 371°C. The tool was designed to impart shear during the injection

process in an attempt to achieve some alignment of the MWCNTs in the flow direction.

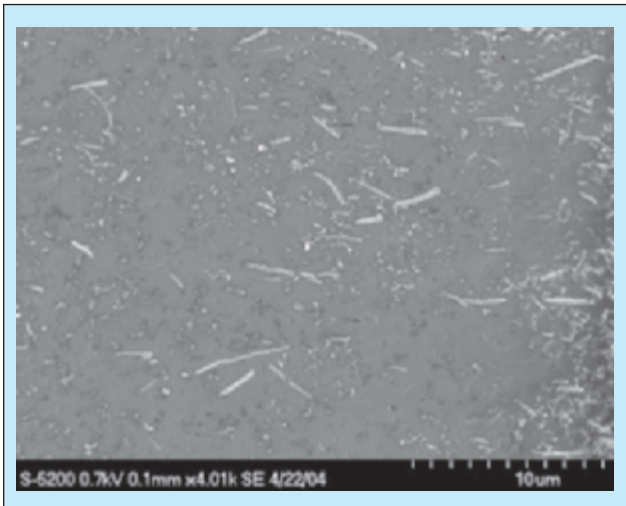
Qualitatively, the moldings from the 10 and 15 weight-percent samples appeared to be good. The moldings were subsequently characterized with respect to thermal, mechanical, and electrical properties. However, as expected from the results of the extrusion experiments, the 20 weight-percent sample could not be injected because of its higher viscosity.

The hardness value of each molded PETI-330/MWCNT specimen was found to be lower than that of the neat resin in the sense that an indenter was found to penetrate to a greater depth or an enhanced plastic deformation of the material was observed. The neat resin specimen was found to be electrically insulating. For the other specimens, the electrical resistivity was found to decrease with increasing concentration of MWCNTs, ranging from $8.86 \times 10^3 \Omega/\text{cm}$ for the 10 weight-percent sample to $5.13 \times$

$10^3 \Omega/\text{cm}$ for the 15 weight-percent sample. The thermal conductivities were found to increase with the proportion of MWCNTs, ranging from 0.219 W/(m·K) for the neat resin specimen to 0.577 W/(m·K) for the 10 weight-percent specimen and 0.777 W/(m·K) for the 15 weight-percent specimen. This trend in thermal conductivity suggests that nanotubes form networks in the polymer matrices that conduct heat, but not to the extent expected based on the high thermal conductivity of the MWCNTs.

Upon machining of the specimens to prepare them for mechanical tests, voids were observed. Unfortunately, these voids made the samples unsuitable for determination of mechanical properties. Notwithstanding the present lack of data on mechanical properties, the electrical and thermal properties and processing characteristics of these materials offer significant potential for applications in which multifunctionality may be required.

*This work was done by John W. Connell, Joseph G. Smith, Emilie J. Siochi, and Dennis C. Working of Langley Research Center; Jim M. Criss of M&P Technologies; Kent A. Watson and Donavon M. Delozier of the National Institute of Aerospace; and Sayata Ghose of the National Research Council. Further information is contained in a TSP (see page 1).
LAR-17082-1*



MWCNTs Were Substantially Aligned along the flow direction after extrusion, as shown in this high-resolution scanning electron micrograph.

Multilayer Impregnated Fibrous Thermal Insulation Tiles

Temperature rises are limited by transpiration cooling.

Ames Research Center, Moffett Field, California

The term “secondary polymer layered impregnated tile” (“SPLIT”) denotes a type of ablative composite-material thermal-insulation tiles having engineered, spatially non-uniform compositions. The term “secondary” refers to the fact that each tile contains at least two polymer layers wherein endothermic reactions absorb considerable amounts of heat, thereby helping to prevent overheating of an underlying structure. These tiles were invented to afford lighter-weight alternatives to the reusable thermal-insulation materials heretofore variously used or considered for use in protecting the space shuttles and other spacecraft from intense atmospheric-entry heating. Tiles of this type could also be useful on Earth as relatively lightweight components of fire-retardant structures.

The SPLIT concept admits to so many different combinations of constituent materials, spatial distributions of the materials, and fabrication processes, that it is not possible to even list, much less summarize or describe all of them. Instead, a representative example must serve to illustrate the main principles. The starting material for fabricating a typical SPLIT is a porous substrate, having a void volume fraction of about 90 percent, that comprises a rigid tile or fabric made from any of a large variety of carbon fibers and/or ceramics fibers. The fiber composition can be the same throughout the thickness or can be graded: for example, it can differ among front, middle, and rear layers.

The front layer, which is the one to be exposed directly to intense heating,

is typically impregnated with a thermosetting resin (e.g., a phenolic or a silicone). This layer becomes the first line of defense against intense heating: a large amount of heat is absorbed in the pyrolysis of the front polymer layer and is dissipated to the environment through a combination of outflow of the pyrolysis gas, and thermal radiation from the char layer formed in the pyrolysis. The outflow of the pyrolysis gas also provides further protection against heating by blocking the inflow of hot ambient gas.

The middle layer (if any) is typically not impregnated. The back layer is the one to be placed in contact or proximity to the structure to be protected. The back layer is initially impregnated with a thermoplastic polymer (the secondary

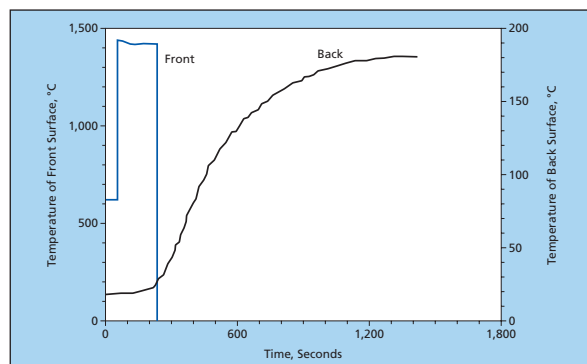
polymer) in solution and the solvent is allowed to evaporate, so that the fibers in the back layer become coated with the thermoplastic but the layer retains substantial porosity. The secondary polymer is chosen to be one that pyrolyzes completely or nearly completely to gaseous products (i.e., leaving little or no solid residue), at a temperature much lower than the pyrolysis temperature of the front layer. For example, polystyrene and poly (methyl methacrylate) decompose at temperatures between 350 and 450 °C.

Eventually, some heat penetrates the front layer and diffuses to the back layer, where the lower-temperature pyrolysis reaction of the secondary polymer retards the transfer of heat to the structure to be protected. The pyrolysis gas from the secondary polymer escapes through the middle (if any) and front layers, thereby effectively preventing excessive heating of the underlying structure

through a combination of transpiration cooling and blockage of inflow of hot ambient gas. With suitable choice of materials and processing, it is possible to delay the onset of heating of the back surface and limit the temperature rise of the back surface (see figure) to a value low enough to protect the underlying structure.

This work was done by Huy K. Tran, Daniel J. Rasky, and Christine E. Szalai of Ames Research Center; Ming-ta S. Hsu of HC Chem Research and Services Corp.; and Joseph A. Carroll of Tether Applications. Further information is contained in a TSP (see page 1).

This invention has been patented by NASA (U.S. Patent No. 6,955,853 B1).



A Pulse of Heat was applied, by an arc jet in a partial vacuum, to the front surface of a 2.73-cm-thick specimen impregnated with a silicone in the front layer and poly (methyl methacrylate) in the back layer. The rear-surface temperature rise, measured by use of thermocouples, was limited to a range that would be safe for an underlying aluminum structure or for most composite-material structures.

Inquiries concerning rights for the commercial use of this invention should be addressed to the Ames Technology Partnerships Division at (650) 604-2954. Refer to ARC-14165-1.



Radiation-Shielding Polymer/Soil Composites

Radiation shields could be fabricated *in situ* at relatively low cost.

Marshall Space Flight Center, Alabama

It has been proposed to fabricate polymer/soil composites primarily from extraterrestrial resources, using relatively low-energy processes, with the original intended application being that habitat structures constructed from such composites would have sufficient structural integrity and also provide adequate radiation shielding for humans and sensitive electronic equipment against the radiation environment on the Moon and Mars. The proposal is a response to the fact that it would be much less expensive to fabricate such structures *in situ* as opposed to transporting them from Earth.

Prototype polymer/soil composite bricks have been fabricated on Earth. Transport calculations have shown that the addition of polymeric materials to

soil significantly improves the radiation-shielding properties of the resulting composites due to the high hydrogen content of the polymeric constituent. Mechanical testing and hypervelocity-ballistic testing of the proposed composites have demonstrated that structural properties can be improved by a factor of 10 when compared to bricks consisting of only the planetary soil.

A typical composite of this type consists of 5-to 95-weight percent polymeric material and 95-to-5-weight percent of the local planetary soil. The polymeric and soil constituents are thoroughly mixed, heated to slightly over the melting point of the polymeric constituent and pressure is applied to ensure complete infiltration of the polymeric mate-

rial within the pores of the soil particles. Through suitable choice of pressure and temperature, the resulting polymer/soil composite can be made nearly free of voids.

This work was done by Subhayu Sen of BAE Systems for Marshall Space Flight Center. Further information is contained in a TSP (see page 1).

In accordance with Public Law 96-517, the contractor has elected to retain title to this invention. Inquiries concerning rights for its commercial use should be addressed to:

BAE Systems

Attn. Subhayu Sen

Subhayu.sen-1@nasa.gov

Refer to MFS-32340-1, volume and number of this NASA Tech Briefs issue, and the page number.

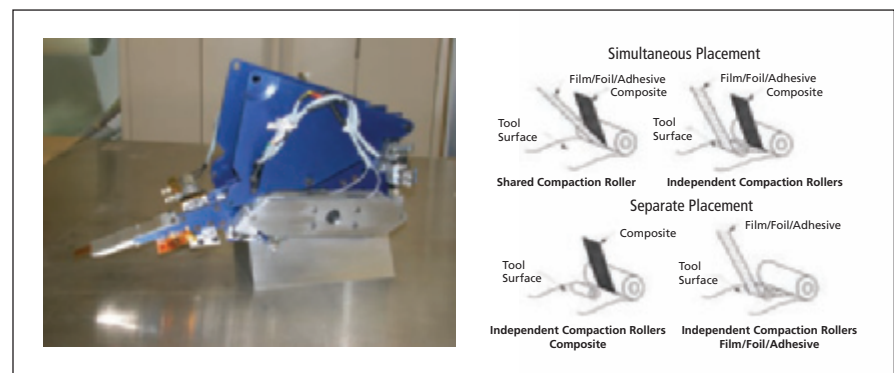
Film/Adhesive Processing Module for Fiber-Placement Processing of Composites

Films, foils, or adhesives may be interleaved while fiber-placing composite material structures.

Marshall Space Flight Center, Alabama

An automated apparatus has been designed and constructed that enables the automated lay-up of composite structures incorporating films, foils, and adhesives during the automated fiber-placement process. This apparatus, denoted a film module, could be used to deposit materials in film or thin sheet form either simultaneously when laying down the fiber composite article or in an independent step. Examples of materials that may be processed with this device include structural core and joining adhesives, permeation barrier films/foils, surfacing films, lightning-strike materials and IVHM (Integral Vehicle Health Monitoring) arrays. The use of this technology will reduce composite fabrication time and will allow for new concepts/designs to be considered for fiber-placed composite structures.

The film module may be easily designed to fit existing fiber-placement ma-



The **Prototype Film Module** is shown on the left. Materials, as shown on the right, may be placed either simultaneously with to the composite tow/tape, or in an independent step such as in the application of external structural core adhesives.

chinery or may be integrally designed into new machines. The film materials may be placed either simultaneously with the fiber composite material as with the case of embedded materials, or in an independent operation as with applica-

tion of exterior structural core adhesives, as shown in the figure. The device is designed such that it may be made to operate by use of existing fiber-placement lay-up program files. This eliminates the need for additional computer

program files to be generated, saving both time and expense.

The film module includes a material supply and feed system, a material preheating system for the tackifying of incoming and substrate materials, and a film-cutting system. The preheating system utilizes an infrared quartz-halogen lamp with a focused parabolic reflector to provide radiant heating of the substrate and incoming materials at the point of application. All prototype device actuators are pneumatic; however, digital

servo/stepper motors may be employed for additional control and accuracy.

The prototype device was designed to supply material of width identical to that of the composite material typically processed by the machine that was used as the test-bed during the course of module development. By thus setting the width of the film, use may be made of the same placement files as written for the composite. The device is designed to be portable and easily removed from the host machine. A simple switch allows

for the disabling of the device when placement of composites alone is being performed.

This work was done by A. Bruce Hulcher of Marshall Space Flight Center. For further information on this technology, contact A. Bruce Hulcher at (256) 544-5124.

This invention is owned by NASA, and a patent application has been filed. For further information, contact Sammy Nabors, MSFC Commercialization Assistance Lead, at sammy.a.nabors@nasa.gov. Refer to MFS-32008-1.

Fabrication of Submillimeter Axisymmetric Optical Components

Surfaces of components can be arbitrarily shaped to optimize spectral responses.

NASA's Jet Propulsion Laboratory, Pasadena, California

It is now possible to fashion transparent crystalline materials into axisymmetric optical components having diameters ranging from hundreds down to tens of micrometers, whereas previously, the smallest attainable diameter was 500 μm . A major step in the fabrication process that makes this possible can be characterized as diamond turning or computer numerically controlled machining on an ultrahigh-precision lathe. This process affords the flexibility to make arbitrary axisymmetric shapes that have various degrees of complexity: examples include a flat disk or a torus supported by a cylinder (see figure), or multiple closely axially spaced disks or tori supported by a cylinder. Such optical components are intended mainly for use as whispering-gallery-mode optical resonators in diverse actual and potential applications, including wavelength filtering, modulation,

photonic generation and detection of microwaves, and research in quantum electrodynamics and quantum optics.

The first step in the fabrication process is to use a brass tube bore with a 30- μm diamond suspension to cut a small cylindrical workpiece from a plate or block of the selected crystalline material. In a demonstration of the process, the cylindrical workpiece was 1.8 mm in diameter and 5 mm long; in general, different dimensions would be chosen to suit a specific application.

The workpiece is then glued to a metal cap that, in turn, is attached to the rotor of an aerostatic spindle. During the rotation of the spindle, a diamond tool is used to cut the workpiece. A computer program is used to control stepping motors that move the diamond tool, thereby controlling the shape cut by the tool. Because the shape can be

controlled via software, it is possible to choose a shape designed to optimize a resonator spectrum.

This work was done by Ivan Grudin, Anatoliy Savchenkov, and Dmitry Strelkov of Caltech for NASA's Jet Propulsion Laboratory. Further information is contained in a TSP (see page 1).

In accordance with Public Law 96-517, the contractor has elected to retain title to this invention. Inquiries concerning rights for its commercial use should be addressed to:

*Innovative Technology Assets Management
JPL*

*Mail Stop 202-233
4800 Oak Grove Drive
Pasadena, CA 91109-8099
(818) 354-2240*

E-mail: iaoffice@jpl.nasa.gov

Refer to NPO-42056, volume and number of this NASA Tech Briefs issue, and the page number.



Electrochemical Disposal of Hydrazines in Water

This method offers advantages of safety, economy, and scalability.

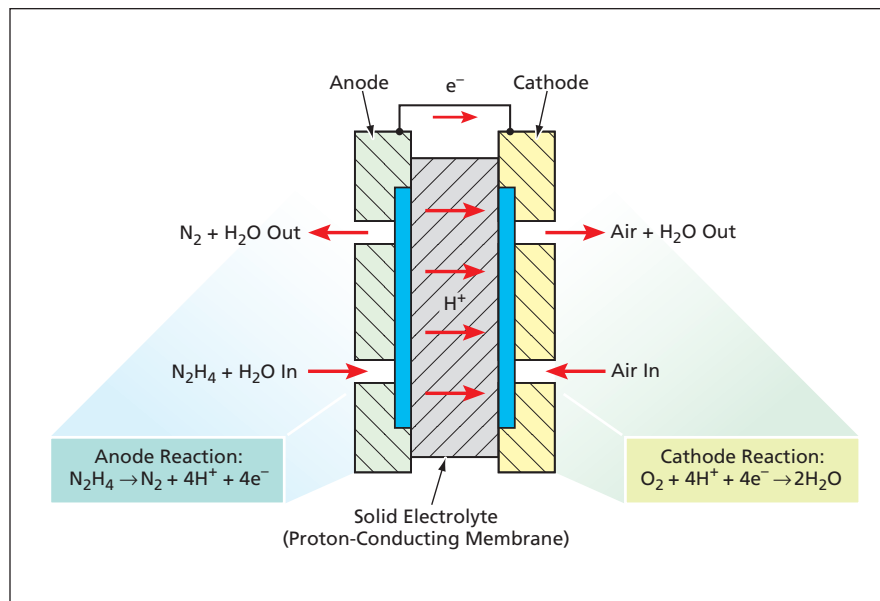
John F. Kennedy Space Center, Florida

An electrochemical method of disposal of hydrazines dissolved in water has been devised. The method is applicable to hydrazine (N_2H_4), to monomethyl hydrazine [also denoted by MMH or by its chemical formula, $(CH_3)HNNH_2$], and to unsymmetrical dimethyl hydrazine [also denoted UDMH or by its chemical formula, $(CH_3)_2NNH_2$]. The method involves a room-temperature process that converts the hydrazine to the harmless products N_2 , H_2O , and, in some cases, CO_2 . In comparison with prior methods of disposing of hydrazines, the present method is safer and less expensive.

Hydrazines are probably best known as hypergolic fuels used in rocket engines. In addition, hydrazines have some industrial uses. The need for safe disposal of hydrazines dissolved in water arises because water is used (1) to clean up spills of these chemicals; (2) to rinse equipment used in storing and transferring them; and (3) as a solvent in gas scrubbers that are typically included in such equipment.

In the present method, one uses an electrochemical cell, which can be operated in either of two modes, depending on the nature of the rinse-water solution(s) to be treated: if the concentration of hydrazine is sufficiently high, the cell can be operated as a fuel cell; otherwise, the cell can be operated as an electrolyzer. The cell (see figure) includes a solid polymer electrolyte sandwiched between electrodes that have three-dimensionally complex, high-surface-area structures and contain appropriate electrocatalysts. The solid polymer electrolyte separates the anodic compartment from the cathodic compartment. Thus, there is no mixing of rinse-water containing hydrazine with any oxidant and, therefore, the undesired formation of nitrogen oxides or nitrate is prevented.

In the anodic compartment, hydrazine is oxidized. Hydrogen ions that are generated in the oxidation of hydrazine travel through the solid electrolyte into the cathodic compartment,



An **Electrochemical Cell** oxidizes highly toxic N_2H_4 to the harmless products N_2 and H_2O . The cell can be operated in an electrolyzer or fuel-cell mode; in either mode, the oxygen needed for oxidation is obtained from the air. The thickness of the proton-conducting membrane is greatly exaggerated here.

where they are converted to hydrogen atoms, which are then oxidized to water, using oxygen from the air. The three-dimensionally complex, high-surface-area electrocatalytic nature of the electrodes promotes the desired chemical reactions, thereby reducing the amount of time needed for treatment, thereby, further, reducing the cost of treatment.

The electrocatalytic materials for the anodic compartment are selected so as to suppress electrochemical reactions (e.g., evolution of oxygen) that are undesired there while promoting the selective oxidation of hydrazine to nitrogen and water (or the selective oxidation of monomethyl hydrazine or unsymmetrical dimethyl hydrazine to nitrogen and carbon dioxide). The electrocatalytic materials for the cathodic compartment are selected to favor the desired oxidation of hydrogen to water. A key feature — essential for successful operation in either the fuel-cell or the electrolyzer mode — is close control of each reaction step through control of the cell current or potential and of the duration of the treatment.

A system for treating hydrazine-contaminated water can easily be scaled up from a single cell to a stack of cells. The system can easily be automated, requires little maintenance, and can be operated without much training. If the concentration of hydrazine is sufficient to enable operation in the fuel-cell mode, then the power generated by the system could offset some or all of the cost of treatment. Even at low concentrations, the cost of treatment — about \$0.03/gallon (about \$0.008/liter) at the time of this report in 2003 — is of the order of a hundredth of the cost of treatment by prior methods.

This work was done by Jinseong Kim, Anuncia Gonzalez-Mar, Carlos Salinas, Laris Rutheford, King-Tsai Jeng, Craig Andrews, and Ratlaya Yalamanchili of Lynntech, Inc., for Kennedy Space Center.

This invention is owned by NASA, and a patent application has been filed. Inquiries concerning nonexclusive or exclusive license for its commercial development should be addressed to the Kennedy Innovative Partnerships Office at (321) 867-8130. Refer to KSC-12133/492.

Statistical Model of Evaporating Multicomponent Fuel Drops

This model overcomes a deficiency of a prior statistical model.

NASA's Jet Propulsion Laboratory, Pasadena, California

An improved statistical model has been developed to describe the chemical composition of an evaporating multicomponent-liquid drop and of the mixture of gases surrounding the drop. The model is intended for use in computational simulations of the evaporation and combustion of sprayed liquid fuels, which are typically mixtures of as many as hundreds of different hydrocarbon compounds. Since an exact model providing a detailed account of all of the compounds would be computationally intractable, the present statistical model is an approximation designed to afford results that are accurate enough to contribute to understanding of the simulated physical and chemical phenomena, without imposing an unduly large computational burden.

As in any model of physical and chemical phenomena, some simplifying assumptions are made: A drop is taken to be a sphere of radius R , wherein the liquid has constant density ρ_l . Evaporation of the liquid is assumed to occur under thermodynamic equilibrium. The gas surrounding the drop — a mixture comprising a carrier gas plus multicomponent vapor from previously evaporated drops — is assumed to obey the perfect-gas equation of state. The gas is postulated to be quasi-steady with respect to the liquid, in the sense that the characteristic time of the gas is much shorter than that of the liquid. Consistent with what would be done in computations involving a very large number of drops, gradients within the drop are neglected; attention is paid only to volumetrically averaged properties represented by the drop temperature and the mass fractions of the chemical species in the drop. The focus on volumetrically averaged drop properties precludes consideration of phenomena

associated with differences among diffusivities of different species.

It is further assumed that the simulated phenomena occur at atmospheric pressure, where solubility of the carrier gas into the liquid is negligible, and that the far field conditions are quiescent. The model includes the applicable equations for the conservation of mass, species, and energy.

The statistical aspect of the model enters through invocation of the concept of continuous thermodynamics, according to which the chemical composition of a fuel is described probabilistically, by use of a probability distribution function (PDF). This concept was summarized in two prior NASA Tech Briefs arti-

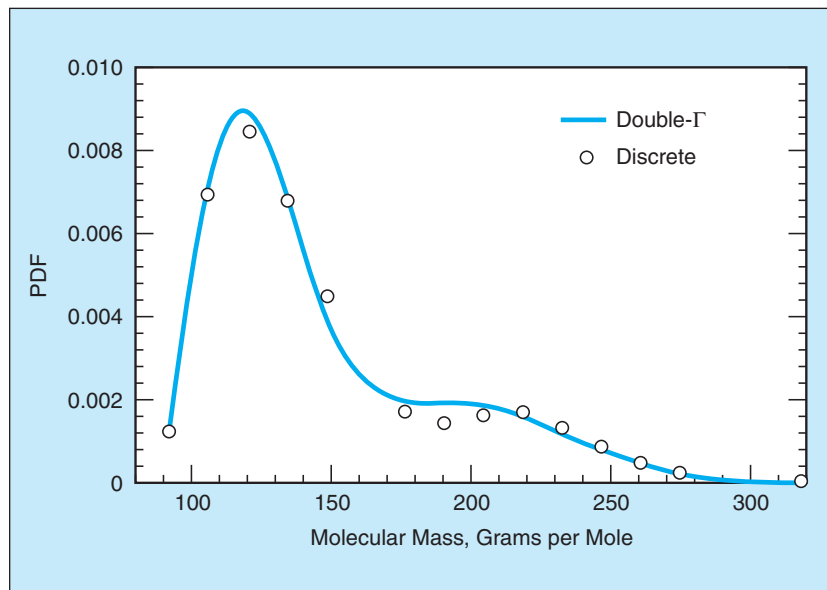
cles: “Model of Mixing Layer With Multicomponent Evaporating Drops” (NPO-30505), Vol. 28, No. 3 (March 2004), page 55, and “Simulations of Evaporating Multicomponent Fuel Drops” (NPO-30641), Vol. 29, No. 3 (March 2005), page 72. However, the present statistical model differs from the model of the cited prior articles.

drop-composition PDF that emerges when condensation of vapor onto drops occurs. The present model generates the needed second peak. The PDF in the present model is a superposition of two Γ -PDFs and, accordingly, is denoted a double- Γ -PDF. It is a function of the molar weight plus five parameters.

Formally, the calculation prescribed by this model can be reduced to an inverse mapping from (1) the first five distribution moments, which can be calculated by use of the conservation equations, to (2) the five parameters of the double- Γ -PDF. The complexity of the inverse mapping, and the fact that the statistics of a discrete-chemical-species model may not be represented exactly by the double- Γ -PDF, make this calculation only approximate.

In a practical calculation, one makes a further approximation by utilizing only the first four moments and four parameters plus a fifth parameter that is determined empirically. Despite these approximations, extensive tests of the model on both diesel oil and gasoline show that the double- Γ -PDF accurately represents the predictions of the discrete-chemical-species model (see figure). Moreover, the mean and variation of composition at the drop surface as computed by use of the double- Γ -PDF are in excellent agreement with those computed by use of the discrete-chemical-species model: this is an important result because these mean and variance determine the composition of the gas mixture.

This work was done by Kenneth Harstad, Patrick Le Clercq, and Josette Bellan of Caltech for NASA's Jet Propulsion Laboratory. Further information is contained in a TSP (see page 1).
NPO-30886



Double- Γ -PDF and Discrete-Model-PDF values were computed for a drop of diesel fuel evaporating at a gas temperature of 600 K. The results shown here are for the time at which a drop has evaporated to one-fifth of its initial mass.

cles: “Model of Mixing Layer With Multicomponent Evaporating Drops” (NPO-30505), Vol. 28, No. 3 (March 2004), page 55, and “Simulations of Evaporating Multicomponent Fuel Drops” (NPO-30641), Vol. 29, No. 3 (March 2005), page 72. However, the present statistical model differs from the model of the cited prior articles.

In the prior model, the PDF is a single-peaked Gamma distribution, which is a function of the molar weight and of several parameters. However, the prior model does not generate a second peak at the low-molar-weight end of the

Resistively Heated SiC Nozzle for Generating Molecular Beams

This nozzle is more durable and efficient relative to its predecessors.

Goddard Space Flight Center, Greenbelt, Maryland

An improved nozzle has been developed to replace nozzles used previously in an apparatus that generates a substantially unidirectional beam of molecules passing through a vacuum at speeds of several kilometers per second. The need to replace the previous nozzles arose from a complex set of causes that can be summarized as follows:

- (1) The previous nozzles had short operational lifetimes because it was necessary to fabricate them from components made of several different materials that, when used together, do not last long at the high operating temperatures needed to generate the requisite high molecular speeds and
- (2) To protect the vacuum chamber from excessive heating, it was necessary to surround the operating nozzle with a cooling shroud that robbed the nozzle of reflected heater power and thereby contributed to energy inefficiency.

The basic principle of operation of the apparatus is the same for both the previous and the present nozzle designs. The main working part of the nozzle is essentially a cylinder that is closed except that there is an inlet for a pressurized gas and, at one end, the cylinder is closed by a disk that contains a narrow central hole that serves as an outlet. The cylinder is heated to increase the thermal speeds of the gas molecules into the desired high-speed range. Heated, pressurized gas escapes through the outlet into a portion of the vacuum chamber that is separated, by a wall, from the rest

of the vacuum chamber. In this portion of the vacuum chamber, the gas undergoes a free jet expansion. Most of the expanded gas is evacuated and thus does not become part of the molecular beam. A small fraction of the expanded beam passes through a narrow central orifice in the wall and thereby becomes a needle-thin molecular beam in the portion of the vacuum on the downstream side of the wall.

In a nozzle of the previous design, the cylinder was made of molybdenum, and the disk with the outlet hole, also made of molybdenum, was welded onto the cylinder at one end. In the improved nozzle, the cylinder and the disk at one end containing the narrow outlet hole are made of a single piece of silicon carbide. In a nozzle of the previous design, the molybdenum cylinder was surrounded by an alumina electrical-insulation cylinder that was, in turn, surrounded by a silicon carbide cylinder that served as an electrical resistance heater. In the improved nozzle, the silicon carbide cylinder serves as its own electrical resistance heater.

In the improved nozzle, the silicon carbide cylinder is brazed to a molybdenum fitting that is brazed to a stainless-steel fitting that is electron-beam welded onto a length of stainless-steel tubing. Electrodes made of tungsten wire are attached to the ends of the silicon carbide cylinder by means of two-piece molybdenum hinge clamps, wherein the electrodes serve as the hinge pins. Sufficient clearance is provided between each molybdenum clamp and the SiC cylin-

der nozzle to accommodate a piece of graphite tape that both cushions and ensures a high degree of electrical contact. To reflect some heater power to the SiC cylinder and thereby both increase energy efficiency and reduce heating of the vacuum chamber, the nozzle as described thus far is surrounded by a radiation shield in the form of 12 concentric cylindrical layers of 50- μ m-thick tungsten foil that are dimpled to maintain gaps between successive layers. The radiation shield is cooled by a circulation subsystem.

The nozzle has been tested using a gas mixture comprising 1 percent argon and 99 percent hydrogen at feed pressures up to 450 psi (\approx 3.1 MPa) and temperatures up to 2,000 °C. In one test at 1,600 °C, the speed of the argon fraction of the beam was observed to be 3.3 km/s. On the basis of performance data from the tests, it has been estimated that the nozzle would have unlimited operational lifetime at room temperature, could operate for many hundreds of hours at 1,000 °C, and could operate for at least 100 hours at 1,500 °C. At operating temperatures above 1,500 °C, the nozzle is vulnerable to clogging, though in the absence of oxygen, it may still be capable of operating for many hours.

*This work was done by Steven Cagiano of Goddard Space Flight Center; Robert Abell of Swales Aerospace; Edward Patrick and Mirl Bendt of Honeywell Technical Services, Inc.; and Cynthia Gundersen of AMU Engineering, Inc. Further information is contained in a TSP (see page 1).
GSC-14837-1.*

Compact Packaging of Photonic Millimeter-Wave Receiver

Bulky positioning mechanisms are not needed.

John H. Glenn Research Center, Cleveland, Ohio

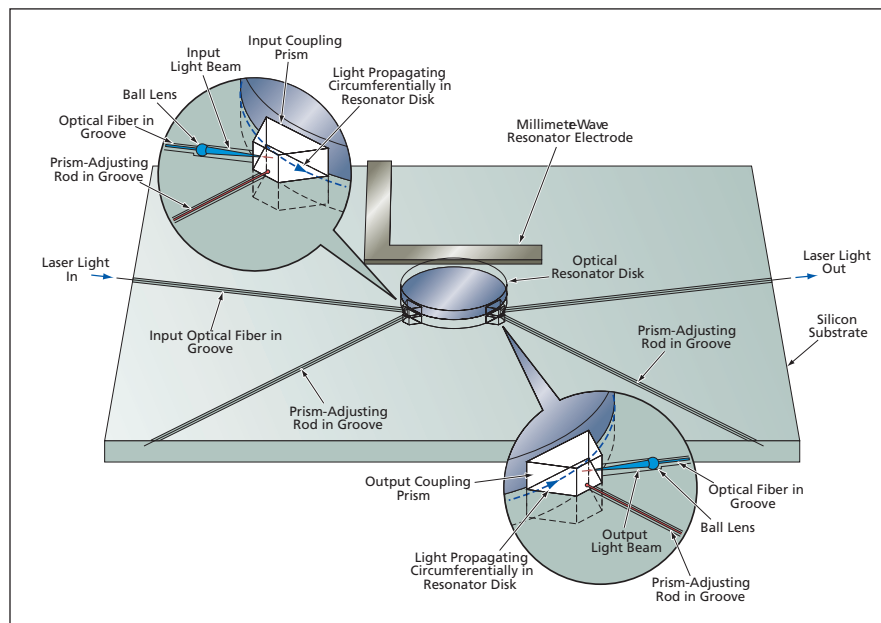
A carrier structure made from a single silicon substrate is the basis of a compact, lightweight, relatively inexpensive package that holds the main optical/electronic coupling components of a photonic millimeter-wave receiver based on a lithium niobate resonator disk. The design of the package is simple and provides for precise relative placement of op-

tical components, eliminating the need for complex, bulky positioning mechanisms like those commonly used to align optical components to optimize focus and coupling. Although a prototype of the package was fabricated as a discrete unit, the design is amenable to integration of the package into a larger photonic and/or electronic receiver system.

The components (see figure) include a lithium niobate optical resonator disk of 5-mm diameter and \approx 200- μ m thickness, positioned adjacent to a millimeter-wave resonator electrode. Other components include input and output coupling prisms and input and output optical fibers tipped with ball lenses for focusing and collimation, respectively.

Laser light is introduced via the input optical fiber and focused into the input coupling prism. The input coupling prism is positioned near (but not in contact with) the resonator disk so that by means of evanescent-wave coupling, the input laser light in the prism gives rise to laser light propagating circumferentially in guided modes in the resonator disk. Similarly, a portion of the circumferentially propagating optical power is extracted from the disk by evanescent-wave coupling from the disk to the output coupling prism, from whence the light passes through the collimating ball lens into the output optical fiber.

The lens-tipped optical fibers must be positioned at a specified focal distance from the prisms. The optical fibers and the prisms must be correctly positioned relative to the resonator disk and must be oriented to obtain the angle of incidence (55° in the prototype) required for evanescent-wave coupling of light into and out of the desired guided modes in the resonator disk. To satisfy all these requirements, precise alignment features are formed in the silicon substrate by use of a conventional wet-etching process. These features include a 5-mm-diameter, 50- μm -deep cavity that holds the disk; two trapezoidal-cross-section recesses for the prisms; and two grooves that hold the optical fibers at the correct positions and angles relative to the prisms and disk. The fiber grooves contain abrupt tapers, near



Optical Components of a millimeter-wave photonic receiver are kept in alignment by mounting them in precise recesses in a silicon substrate.

the prisms, that serve as hard stops for positioning the lenses at the focal distance from the prisms.

There are also two grooves for prism-adjusting rods. The design provides a little slack in the prism recesses for adjusting the positions of the prisms by means of these rods to optimize the optical coupling.

This work was done by Hung Nguyen, John Pouch, and Felix Miranda of Glenn

Research Center, and Anthony F. Levi of the University of Southern California. Further information is contained in a TSP (see page 1).

Inquiries concerning rights for the commercial use of this invention should be addressed to NASA Glenn Research Center, Innovative Partnerships Office, Attn: Steve Fedor, Mail Stop 4-8, 21000 Brookpark Road, Cleveland, Ohio 44135. Refer to LEW-17694-1.

Diffraction Combiner of Single-Mode Pump Laser-Diode Beams Multiple beams can be combined without inducing multifrequency lasing.

NASA's Jet Propulsion Laboratory, Pasadena, California

An optical beam combiner now under development would make it possible to use the outputs of multiple single-mode laser diodes to pump a neodymium: yttrium aluminum garnet (Nd:YAG) non-planar ring oscillator (NPRO) laser while ensuring that the laser operates at only a single desired frequency. Heretofore, an Nd:YAG NPRO like the present one has been pumped by a single multimode laser-diode beam delivered via an optical fiber. It would be desirable to use multiple pump laser diodes to increase reliability beyond that obtainable from a single pump laser diode. However, as explained below, simplistically coupling multiple multimode laser-diode beams through a fiber-optic combiner would entail a significant reduction in cou-

pling efficiency, and lasing would occur at one or more other frequencies in addition to the single desired frequency.

Figure 1 schematically illustrates the principle of operation of a laser-diode-pumped Nd:YAG NPRO. The laser beam path is confined in a Nd:YAG crystal by means of total internal reflections on the three back facets and a partial-reflection coating on the front facet. The wavelength of the pump beam — 808 nm — is the wavelength most strongly absorbed by the Nd:YAG crystal. The crystal can lase at a wavelength of either 1,064 nm or 1,319 nm — which one depending on the optical coating on the front facet. A thermal lens effect induced by the pump beam enables stable lasing in the lowest-order transverse

electromagnetic mode (the TEM_{00} mode). The frequency of this laser is very stable because of the mechanical stability of the laser crystal and the unidirectional nature of the lasing. The unidirectionality is a result of the combined effects of (1) a Faraday rotation induced by an externally applied magnetic field and (2) polarization associated with non-normal incidence and reflection on the front facet.

In order to restrict lasing to a single frequency, it is necessary to confine the pump beam within the region occupied by the TEM_{00} mode of the NPRO laser beam near the front facet inside the crystal. In practice, this means that the pump beam must be focused to within a given solid angle (Ω) and area (A). [If a

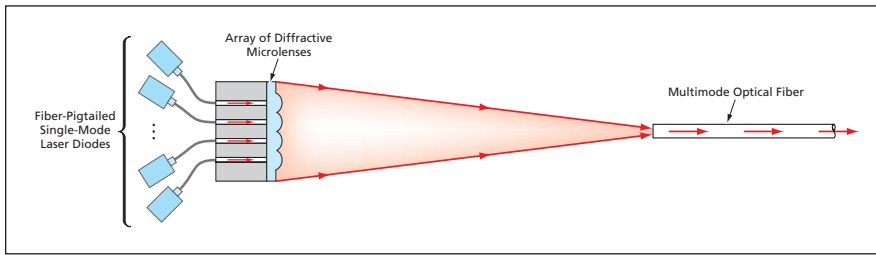


Figure 2. **Multiple Single-Mode Laser-Diode Beams** are focused onto a single narrow spot by use of an array of diffractive microlenses.

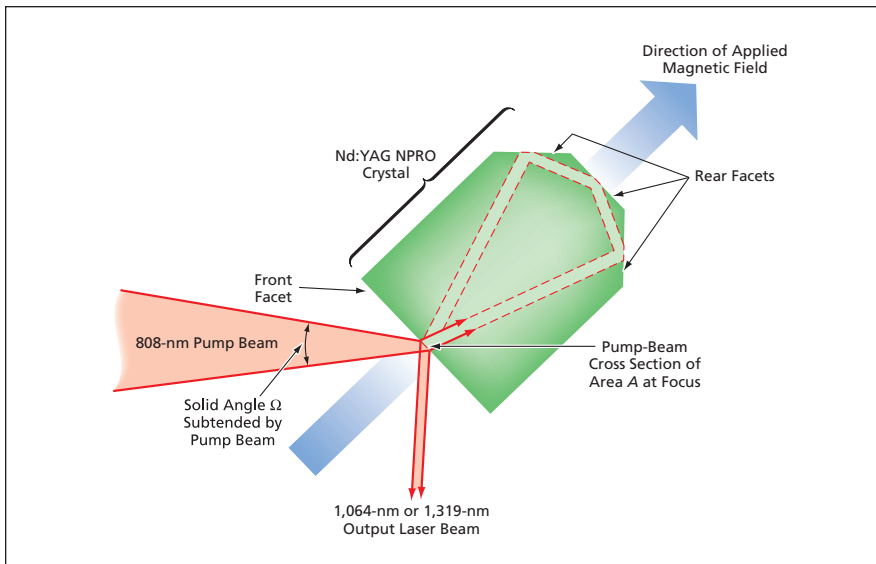


Figure 1. A **Pump Beam of Solid Angle Ω** has a cross section of area A at incidence upon the front facet of an Nd:YAG NPRO laser crystal.

given pump beam has a larger A or larger Ω but its $A\Omega$ is equal to or less than the maximum $A\Omega$ for single-frequency lasing in the crystal, then an imaging lens can be used to trade A against Ω so that both A and Ω are equal to or smaller than the maximum values for single-frequency lasing. It is possible to do this because it is a basic principle of optics that $A\Omega$ is preserved in imaging by a lens.]

The $A\Omega$ of a commercial multimode 808-nm laser diode of the type used

heretofore is not axisymmetric: instead, it is elliptically distributed about the optical axis and, hence, does not match the circular distribution of a multimode fiber of the type used heretofore to deliver a pump beam. As a result of this mismatch, $A\Omega$ for the pump beam emerging from the output end of the fiber is increased, typically to near the maximum single-frequency-lasing value in at least one of the planes containing the principal axes of the elliptical distribution. Consequently, it is difficult or

impossible to maintain single-frequency lasing when combining the beams from two or more multimode laser diodes.

In the present approach (see Figure 2), the beams from multiple fiber-pigtailed single-mode laser diodes are coupled to single-mode optical fibers that have been placed together in a hexagonal-close-packing planar array. An array of diffractive microlenses, custom-designed and fabricated on a glass substrate by electron-beam lithography, is placed in front of the fiber array. The custom design and position of the lens array are chosen, according to the precisely measured actual positions of the fibers, so that the single-mode beams emerging from all the single-mode optical fibers are focused on the same small circular spot centered on the input face of a suitable multimode optical fiber. In use, the beam emerging from the output end of the multimode fiber would be focused onto the front facet of an Nd:YAG NPRO crystal in the usual way. It is anticipated that the $A\Omega$ of the pump light thus incident on the crystal would be less than the maximum single-frequency-lasing value.

This work was done by Duncan Liu, Daniel Wilson, Yueming Qiu, and Siamak Forouhar of Caltech for NASA's Jet Propulsion Laboratory. Further information is contained in a TSP (see page 1).

In accordance with Public Law 96-517, the contractor has elected to retain title to this invention. Inquiries concerning rights for its commercial use should be addressed to:

*Innovative Technology Assets Management
JPL*

*Mail Stop 202-233
4800 Oak Grove Drive
Pasadena, CA 91109-8099
(818) 354-2240*

E-mail: iaoffice@jpl.nasa.gov

Refer to NPO-42411, volume and number of this NASA Tech Briefs issue, and the page number.

Wide-Band, High-Quantum-Efficiency Photodetector

This device could detect single photons.

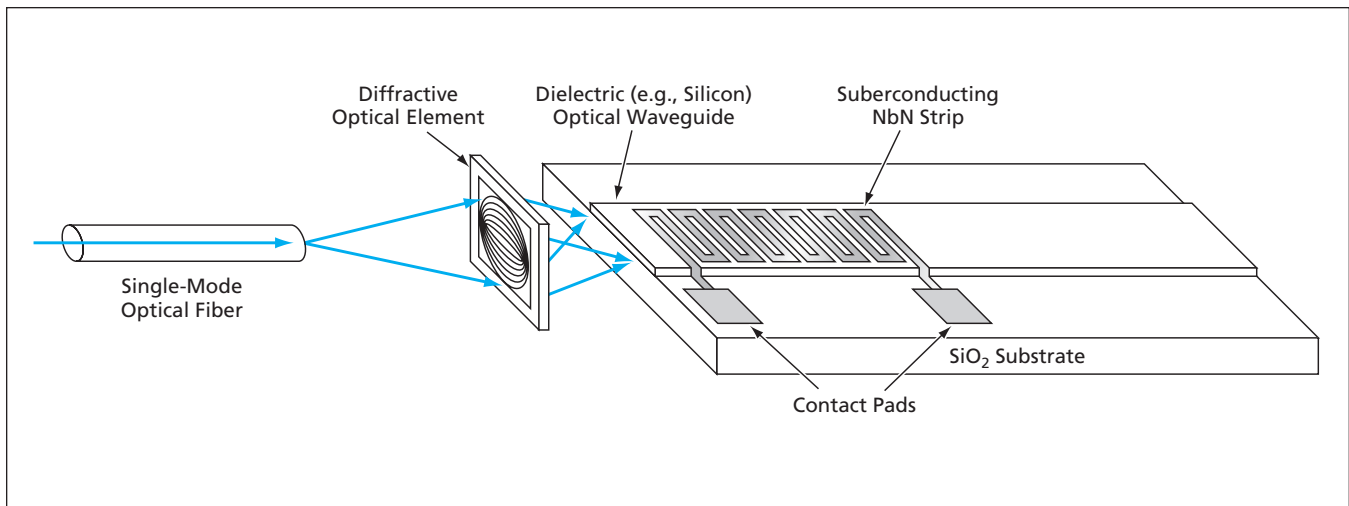
NASA's Jet Propulsion Laboratory, Pasadena, California

A design has been proposed for a photodetector that would exhibit a high quantum efficiency (as much as 90 percent) over a wide wavelength band, which would typically be centered at a wavelength of 1.55 μm . This and similar photodetectors would afford a capability

for detecting single photons — a capability that is needed for research in quantum optics as well as for the practical development of secure optical communication systems for distribution of quantum cryptographic keys.

The proposed photodetector would

be of the hot-electron, phonon-cooled, thin-film superconductor type. The superconducting film in this device would be a meandering strip of niobium nitride. In the proposed photodetector, the quantum efficiency would be increased through incorporation of opti-



Input Light Would Be Focused Into a Waveguide, where it would propagate along, and interact with, a meandering superconducting strip made of niobium nitride.

cal components, described below, that would increase the electromagnetic coupling between the input optical field and the meandering superconducting film.

The meandering niobium nitride strip would be fabricated on top of a dielectric (e.g., silicon) optical waveguide on a silicon dioxide substrate (see figure). The input end face of the waveguide would be cut, polished, and antireflection-coated to maximize in-coupling efficiency. The thickness of the waveguide would be chosen so that at the design wavelength, there would be a single through-the-thickness electromagnetic mode, the evanescent tail of which would overlap with the niobium nitride strip. Because the waveguide would exhibit little optical loss

over the length of the strip, there would be a high probability of absorption of photons by the strip. The width of the waveguide would be chosen to accommodate multiple widthwise electromagnetic modes, thereby increasing the interaction of light with the niobium nitride strip.

Light would be brought to the photodetector via an optical fiber. A point-to-line-focusing diffractive optical element would couple the light from the output end of the optical fiber into the waveguide. The diffractive optical element would be specially designed and fabricated to collimate as well as possible in the width dimension and to focus as well as possible in the thickness dimension in order to maximize the coupling into the desired waveguide electromagnetic mode.

This work was done by Deborah Jackson, Daniel Wilson, and Jeffrey Stern of Caltech for NASA's Jet Propulsion Laboratory. Further information is contained in a TSP (see page 1).

In accordance with Public Law 96-517, the contractor has elected to retain title to this invention. Inquiries concerning rights for its commercial use should be addressed to:

*Innovative Technology Assets Management
JPL*

Mail Stop 202-233

4800 Oak Grove Drive

Pasadena, CA 91109-8099

(818) 354-2240

E-mail: iaoffice@jpl.nasa.gov

Refer to NPO-40163, volume and number of this NASA Tech Briefs issue, and the page number.



➤ A Robustly Stabilizing Model Predictive Control Algorithm

The algorithm can be applied to industrial and automotive systems.

NASA's Jet Propulsion Laboratory, Pasadena, California

A model predictive control (MPC) algorithm that differs from prior MPC algorithms has been developed for controlling an uncertain nonlinear system. This algorithm guarantees the resolvability of an associated finite-horizon optimal-control problem in a receding-horizon implementation. Given a feasible solution to the finite-horizon optimal control problem at an initial time, resolvability implies the ability to solve the optimal control problem at subsequent times.

Originally developed for the control of spacecraft in the proximity of small celestial bodies, the algorithm can also be applied to other systems (such as industrial and automotive systems) for which robust feedback control may be required. The algorithm consists of a feedforward and a feedback component. The feedforward part is computed by

the on-line solution of the finite-horizon optimal control problem with the nominal system dynamics, with a relaxation of the initial state constraint at each computation.

The feedback component makes this relaxation possible, which in turn guarantees resolvability and asymptotic stability once an initial feasible solution is obtained at the start of a maneuver. The feedback part involves off-line design of a feedback control policy based on the uncertainty bounds in the dynamical model of the system. Consequently, this algorithm is robust to system uncertainties that are explicitly accounted for in the design of the feedback portion of the control input.

This explicit characterization of the robustness to the uncertainties (which can easily be extended to external disturbances) is particularly desirable in a real-

time autonomous control application. Furthermore, the ability to solve for an open-loop trajectory during a maneuver enables model updates (possibly based on real-time information) into the control problem to reduce model uncertainty and improve optimality for the open-loop trajectory. The algorithm has been shown to be robustly stabilizing under state and control constraints with a region of attraction composed of initial states for which solution of the finite-horizon optimal control problem is feasible.

This work was done by A. Behçet Açkmeçe and John M. Carson III of Caltech for NASA's Jet Propulsion Laboratory. Further information is contained in a TSP (see page 1).

The software used in this innovation is available for commercial licensing. Please contact Karina Edmonds of the California Institute of Technology at (626) 395-2322. Refer to NPO-42754.

➤ Modeling Evaporation of Drops of Different Kerosenes

One model applies to all three classes of hydrocarbon constituents.

NASA's Jet Propulsion Laboratory, Pasadena, California

A mathematical model describes the evaporation of drops of a hydrocarbon liquid composed of as many as hundreds of chemical species. The model is intended especially for application to any of several types of kerosenes commonly used as fuels. Like evaporating-multi-component-fuel-drop models described in several previous *NASA Tech Briefs* articles, the present model invokes the concept of continuous thermodynamics, according to which the chemical composition of the evaporating multi-component liquid is described by use of a probability distribution function (PDF). However, as described below, the present model is more generally applicable than is its immediate predecessor.

The present model is built on the one reported in "Statistical Model of Evaporating Multicomponent Fuel Drops" (NPO-30886), which appears elsewhere

in this issue. To recapitulate: The PDF in that model is a superposition of two functions and, accordingly, is denoted a double PDF. It is a function of the molecular weight plus five other parameters. Unfortunately, some of those other parameters depend on the class of homologous hydrocarbon species, so that it becomes necessary to have a double PDF for each such class entering the fuel composition. The introduction of multiple double PDFs would make the computation very cumbersome, negating the advantage of the continuous-thermodynamics formulation. The derivation of the present model is driven by the concept of a unified thermodynamic representation of three classes of homologous hydrocarbons (alkanes, naphthenes, and aromatics) that constitute the principal components of kerosenes. Somewhat more specifically, it is sought to characterize

the hydrocarbons in each homologous series by unified reference temperatures, pressures, and other parameters that depend only on molecular weights and thermodynamic quantities.

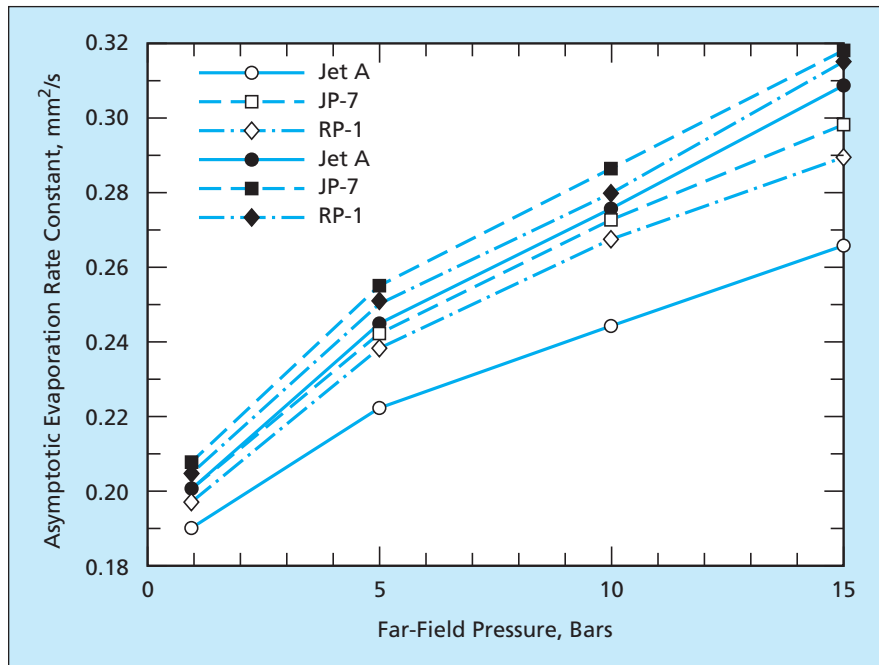
The derivation leads to a new version of the double PDF, in which the square root of the molecular weight occupies the position previously occupied by the molecular weight and other parameters are modified accordingly. By design, this version of the double PDF applies to the three major homologous series in kerosene; hence, it is not necessary to use multiple double PDFs. An additional advantage of this formulation is that it is valid over the subcritical region in the pressure range from 1 to 15 bars (0.1 to 1.5 MPa).

The model has been tested on three kerosenes used as aircraft and rocket fuels: Jet A, JP-7, and RP-1. The present

version of the double PDF has been fitted to the discrete species distributions of these kerosenes and extensive calculations of evaporation of isolated drops performed. The results show that under the assumption of a quasi-steady gas phase, a

relation known in the literature as the D^2 law (pertaining to the rate of decrease of the square of the drop diameter) is recovered after an initial drop-heating transient. A related quantity known in the literature as the asymptotic evaporation rate constant has been found to be an increasing function of the far-field temperature and pressure, a complex function of far-field composition, and a weak function of the difference between the drop-surface and far-field vapor molar fractions. In a comparison between results obtained (a) under the assumption that the interior of the drop is well mixed (the "wm" assumption) and (b) under the assumption that the drop can evaporate either in a well-mixed mode or at unchanging (frozen) composition (the "wm-fc" assumption), it was found that the differences between the asymptotic evaporation rate constants under the two assumptions is within the range of uncertainty in the transport properties (see figure).

This work was done by Josette Bellan and Kenneth Harstad of Caltech for NASA's Jet Propulsion Laboratory. Further information is contained in a TSP (see page 1).
NPO-40437



The **Asymptotic Evaporation Rate Constants** of three kerosenes as a function of far-field pressure were computed for a far-field temperature of 1,000 K and zero far-field vapor fraction.



Development of Vapor-Phase Catalytic Ammonia Removal System

A report describes recent accomplishments of a continuing effort to develop the vapor-phase catalytic ammonia removal (VPCAR) process for recycling wastewater for consumption by humans aboard a spacecraft in transit to Mars. The VPCAR process is implemented by a system of highly integrated design in which some power consumption is accepted as a cost of minimizing the volume and mass of a wastewater-processing system and eliminating the need to resupply water. The core of the system is a wiped-film rotating-disk (WFRD) evaporator, which removes inorganic salts and nonvolatile organic compounds from the wastewater stream and concentrates these contaminants into a recycle-and-bleed stream. The WFRD evaporator is also part of a subsystem that distills water from the wastewater stream. This subsystem operates in a vacuum-vapor/compression distillation configuration in the temperature range from 20 to 65 °C. Volatile organic compounds and ammonia, distilled along with water, are oxidized to CO₂, H₂O, and N₂O in a packed-bed, high-temperature catalytic reactor placed at the outlet of the vapor-phase compressor of the distillation subsystem. A VPCAR engineering demonstration unit is expected to be included in a human-rated simulation of a mission to Mars.

This work was done by Michael Flynn, John Fisher, and Mark Kliss of Ames Research Center; Bruce Borchers of Orbital Sciences Corp.; Badawi Tleimat and Maher Tleimat of Water Reuse Technology Inc.; and Gregory Quinn, James Fort, Tim Nalette, Gale Baker, and Joseph Genovese of Hamilton Sundstrand Space Systems International, Inc. Further information is contained in a TSP (see page 1).

Inquiries concerning rights for the commercial use of this invention should be addressed to the Ames Technology Partnerships Division at (650) 604-2954. Refer to ARC-14607-1.

Several Developments in Space Tethers

Five reports address different aspects of development of tethers to be deployed from spacecraft in orbit around the

Earth. The first report discusses proposed optoelectronic tracking of retroreflective objects located at intervals or of retroreflective coats along the entire length of a tether to measure lateral motions. The second report describes digitally controlled spooling machinery that retracts or extends a tape tether at controlled speed and tension in the spool isolated from uncontrolled tension on the outside. The third report discusses part of this machinery that pivots to accommodate misalignments between the deployed and spooled portions of the tether and contains rollers used to exert tension and speed control. The fourth report discusses aspects of designs of proposed electrodynamic tethers, which would be electrically conductive and would interact with the magnetic field of the Earth to exert forces to modify orbits of deploying spacecraft. The fifth report discusses electrical aspects of designs of electrodynamic tape tethers, including the use of solar cells or motional electromagnetic force to generate currents in tethers and the use of electron emitters and electron and ion collectors at opposite ends of tethers to make electrical contact with the thin plasma in surrounding space.

This work was done by Andrew Santangelo and Rich Sturmfels of The Michigan Technic Corp. and Neal Rothwell of Double R Controls for Marshall Space Flight Center. Further information is contained in a TSP (see page 1).

MFS-31822/4/6/7/30

Design Concept for a Nuclear Reactor-Powered Mars Rover

A report presents a design concept for an instrumented robotic vehicle (rover) to be used on a future mission of exploration of the planet Mars. The design incorporates a nuclear fission power system to provide long range, long life, and high power capabilities unachievable through the use of alternative solar or radioisotope power systems. The concept described in the report draws on previous rover designs developed for the 2009 Mars Science laboratory (MSL) mission to minimize the need for new technology developments.

The surface fission power system that would be used consists of a 15 kW (thermal) heat-pipe-cooled reactor coupled

with a Stirling generator to provide 3 kW of electrical power. This power system would be compact enough to fit readily into prior rover chassis concepts, allowing further adaptation of previously designed MSL elements, including the aeroshell and pallet lander system, with modifications to support the significant mass added by the nuclear reactor and its associated shielding. The estimated mass of the fission power system, including its mission-specific shielding, is 1,169 kg.

This work was done by John Elliott of Caltech, Dave Poston of Los Alamos National Laboratory, and Ron Lipinski of Sandia National Laboratory for NASA's Jet Propulsion Laboratory. Further information is contained in a TSP (see page 1). NPO-30865

Formation-Initialization Algorithm for N Spacecraft

A paper presents an algorithm to initialize a formation of N distributed spacecraft in deep space. Such formations will enable variable-baseline interferometers in future NASA missions designed to study the structure and origin of the universe. The algorithm described in the paper reflects some basic assumptions:

1. Each spacecraft is capable of omnidirectional radio communication with any other spacecraft,
2. Each spacecraft is equipped with a limited field-of-view sensor relative position sensor (RPS) to measure the relative positions and velocities of other formation members, and
3. Spacecraft maneuvers must satisfy Sun-angle pointing constraints to shield sensitive optical equipment from direct sunlight.

The formation initialization algorithm proceeds by first dividing the spacecraft into two groups with anti-parallel RPS sensor boresights. Next, the spacecraft perform a three-phase (in-plane, out-of-plane, and near-field) sky search involving synchronized maneuvers to ensure full sky coverage while maintaining front-to-front, simultaneous RPS sensor lock. During the sky search, the spacecraft are grouped into two classes of sub-formations. The initialization problem is then reduced to the simpler problem of joining the sub-formations. The paper includes an analytical

proof that the algorithm is guaranteed to initialize the formation as required.

This work was done by Scott Ploen, Daniel Scharf, and Fred Hadaegh of Caltech for NASA's Jet Propulsion Laboratory. Further information is contained in a TSP (see page 1).

The software used in this innovation is available for commercial licensing. Please contact Karina Edmonds of the California Institute of Technology at (626) 395-2322. Refer to NPO-43040.



DNSs of Multicomponent Gaseous and Drop-Laden Mixing Layers Achieving Transition to Turbulence

A paper describes direct numerical simulations (DNSs) of three-dimensional mixing-layer flows undergoing transition to turbulence; the mixing layers may or may not be laden with evaporating liquid drops. In contrast to most studies in this field, the general case is

investigated here where both the gas and the liquid drops' composition encompasses a very large number of species. The simulations were performed using a mathematical model discussed in several prior NASA Tech Briefs articles; the prior studies described a laminar mixing layer, whereas the present study describes a mixing layer that has all attributes of turbulence. The model includes governing equations in an Eulerian and a Lagrangian reference frame for the gas and drops, respectively. To mathematically describe the myriad of species, the model relies on continuous thermodynamics concepts. The paper succinctly reiterates the model and discusses results of the new numerical simulations. Comparisons are performed with previous single-species similar simulations and with the laminar simulations using the same model. The paper presents several conclusions, the main one being that differences be-

tween single- and multi-species turbulent flows having the same initial conditions are so significant that neither experiments on, nor theoretical studies of, single-species flows are adequate as surrogates for studies of multi-species flows.

This work was done by Josette Bellan and Laurent Selle of Caltech for NASA's Jet Propulsion Laboratory. Further information is contained in a TSP (see page 1).

In accordance with Public Law 96-517, the contractor has elected to retain title to this invention. Inquiries concerning rights for its commercial use should be addressed to:

Innovative Technology Assets Management

JPL

Mail Stop 202-233

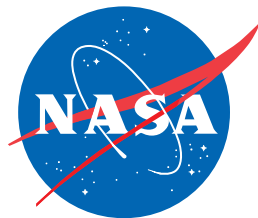
4800 Oak Grove Drive

Pasadena, CA 91109-8099

(818) 354-2240

E-mail: iaoffice@jpl.nasa.gov

Refer to NPO-42632, volume and number of this NASA Tech Briefs issue, and the page number.



National Aeronautics and
Space Administration